

Optimization of chitosan-based nanosystems to deliver plasmid DNA vaccines

Carlos Afonso Rodolfo

Dissertação para obtenção do Grau de Mestre em
Bioquímica
(2^o ciclo de estudos)

Orientador: Prof. Doutor Ângela Maria Almeida de Sousa
Co-orientador: Prof. Doutor Diana Rita Barata Costa
Co-orientador: Prof. Doutor Helena Isabel Fialho Florindo Roque Ferreira

Janeiro de 2022

Agradecimentos

Ao elaborar esta dissertação de mestrado, posso afirmar que este foi um dos projetos mais desafiantes a nível psicológico com que me deparei até ao momento. Por este motivo estou muito agradecido a todos aqueles que me ajudaram e estiverem a meu lado na sua realização.

Em primeiro lugar gostava de agradecer aos meus pais Ana e Joaquim Rodolfo, por me proporcionarem esta oportunidade, por todo o apoio que me deram nos bons e nos maus momentos, por toda compreensão e paciência que tiveram ao longo deste percurso. Agradecer também como festejámos e comemorámos todas as pequenas vitórias que ia alcançando ao longo do mesmo!

Quero também agradecer á Professora Doutora Ângela Sousa, à Professora Doutora Diana Costa e à Professora Doutora Helena Ferreira pela oportunidade de realizar este projeto. Agradeço toda a paciência e tempo que despenderam para me ajudar ao longo do mesmo. Toda a orientação e conhecimento científico partilhado foi muito importante para a realização deste trabalho.

À Universidade da Beira Interior e ao Centro de Investigação em Ciências da Saúde pela disponibilização de todas as condições necessárias à realização desta dissertação.

Agradeço também a todos os colegas de laboratório que me ajudaram e partilharam comigo o seu conhecimento. O meu muito obrigado à Dalinda, Dianas, Raquel, Tânia e Bruno. Um agradecimento especial à Cathy, à Sofia e ao Renato com quem guardo muitos momentos divertidos e que sempre estiveram presentes para me apoiar.

Quero agradecer à minha família da Covilhã, Carlos, Rui, João e Nicolas. Agradeço por todos os bons momentos que passámos enquanto fomos estudantes da UBI, levo na memória muito boas recordações, assim como grandes amizades. O vosso apoio foi muito importante para atravessar este obstáculo.

Por fim agradeço ao meu grande amigo de sempre João Pedro pelo apoio e por todas as chamadas/mensagens. Foi bom saber que podemos sempre contar com um bom amigo mesmo estando a muitos quilómetros de distância.

Resumo alargado

O cancro é a segunda causa de morte a nível mundial e estima-se que, num futuro próximo, poderá tornar-se a primeira. O cancro do colo do útero é o quarto cancro mais comum entre as mulheres em todo o mundo, e em países pouco desenvolvidos, chega a ser o que tem a maior incidência entre as mulheres. Este tipo de cancro é causado, na maioria das vezes, pelo Vírus do Papiloma Humano (HPV). A incidência deste cancro diminuiu em países com bons sistemas de saúde devido a um programa de vacinação e prevenção contra este vírus. As vacinas administradas atualmente são baseadas em partículas semelhantes a vírus, construídas a partir da expressão recombinante da proteína L1, que pertence ao capsídeo do HPV. No entanto, estas vacinas são apenas preventivas, não tendo qualquer efeito terapêutico caso a vacina seja administrada a uma pessoa que tenha contraído previamente a infeção.

Atualmente, as vacinas de ADN têm sido uma ferramenta inovadora com grande potencial para ajudar na batalha contra infeções virais, ou provenientes de outros agentes patogénicos, e contra vários tipos de cancro. Para entregar o ADN às células eucarióticas, deve ser criado um sistema de entrega para proteger, transportar e entregar o ADN à célula-alvo. As vacinas de ADN têm como objetivo codificar genes, característicos dos agentes patogénicos ou de células cancerígenas, de forma a ativar e gerar respostas imunitárias específicas. Neste contexto, o desenvolvimento de uma vacina de ADN que codifica a oncoproteína E7 do HPV pode ser uma ferramenta eficaz contra o cancro do colo do útero, induzido pela infeção do vírus HPV, devido aos seus potenciais efeitos preventivos e terapêuticos. Esta oncoproteína é responsável por interferir com a proteína do retinoblastoma, que por sua vez, desempenha funções na regulação do ciclo celular das células eucarióticas. Para maximizar a eficiência destas vacinas, é fundamental o desenvolvimento de um sistema de entrega adequado.

Assim, o presente trabalho baseou-se na otimização da formulação de sistemas de entrega baseados no polímero de quitosano, tendo sido explorados quatro tipos de quitosano com diferentes pesos moleculares: quitosano de alto peso molecular (HMW, 200-500 kDa), baixo peso molecular (LMW, 50-190 kDa), 20 kDa e 5 kDa. A técnica utilizada para formular os sistemas foi a gelificação iónica, baseada em *ionic crosslinking*. A formulação dos sistemas ocorreu pela interação entre os polímeros de quitosano, que apresentam carga positiva, o *crosslinker* tripolifosfato de sódio (TPP) e o ADN plasmídico (pADN), codificando E7 mutado, que apresentam carga negativa. A

inclusão do TPP teve como objetivo compactar as nanopartículas formadas e aumentar a sua estabilidade, conferindo uma forma esférica mais definida. Para conseguir otimizar a formulação dos sistemas de entrega com cada polímero explorado, foi utilizada uma ferramenta de desenho de experiências (DoE). Esta ferramenta permitiu combinar vários parâmetros/inputs em simultâneo (concentrações de quitosano e TPP) para obter as condições ótimas de formulação dos sistemas com base nas respostas escolhidas (tamanho, índice de polidispersividade (PDI) e potencial zeta), de modo a realizar o mínimo número de experiências possível. Após a realização dos ensaios propostos e caracterização das propriedades das formulações obtidas, foram introduzidas as respetivas respostas no programa de DoE e realizada uma análise estatística. Os modelos lineares e quadráticos obtidos foram estatisticamente significativos (p -valor $<0,05$) e o “lack of fit” não significativo, com coeficiente de determinação adequado. Todos os pontos ótimos previstos para cada polímero de quitosano foram validados com sucesso.

Posteriormente, outros estudos foram conduzidos para avaliar as propriedades dos sistemas de entrega formulados com as condições definidas nos pontos ótimos. Foram realizadas análises de microscopia eletrónica de varrimento (SEM) para avaliar a morfologia, espectroscopia de infravermelhos da transformada por Fourier para avaliar as propriedades químicas e grupos funcionais específicos, diferentes ensaios de estabilidade para avaliar a resistência e a libertação de ADN, e por último, ensaios de citotoxicidade para assegurar a biocompatibilidade das nanopartículas de quitosano. Os quatro sistemas de entrega desenvolvidos apresentavam características satisfatórias, sendo constituídos por nanopartículas esféricas ou ovais, as quais apresentavam boa estabilidade e resistência, retenção de ADN e boa biocompatibilidade.

Neste sentido, a ferramenta DoE revelou ser uma ferramenta adequada para explorar e adaptar as características dos nanosistemas quitosano/TPP/pADN, contribuindo significativamente para desenvolver um sistema com propriedades adequadas de encapsulação, transporte e entrega de um pADN, proporcionando assim um avanço no campo de pesquisa da entrega de vacinas de ADN.

Palavras-chave

Desenho de experiências; HPV; polímeros de quitosano; sistemas de entrega; vacina de ADN.

Abstract

Cancer is the second leading cause of death worldwide and it is estimated that soon it could become the first. Cervical cancer is the fourth most common cancer among women worldwide and in underdeveloped countries, it is the most common cancer among women. This cancer is most often caused by the Human Papilloma Virus (HPV). The incidence of this cancer has decreased in countries with good health systems due to a vaccination and prevention programme against this virus. Currently, vaccines are based on virus-like particles constructed from the recombinant expression of the L1 protein, which belongs to the HPV capsid. However, existing vaccines are only preventive and have no therapeutic effect if the vaccine is administered to a person who has previously contracted the infection.

Currently, DNA vaccines constitute an innovative tool with great potential to help in the battle against viral infections or from other pathogens, and against various types of cancer. To deliver the DNA to eukaryotic cells, a delivery system must be created to protect, transport and deliver the DNA to the target cells. DNA vaccines aim to encode genes, characteristic of pathogens or cancer cells, in order to activate and generate specific immune responses. In this context, the development of a DNA vaccine encoding the HPV E7 oncoprotein, responsible for interfering with the tumour suppressor retinoblastoma protein, which is responsible for regulating the cell cycle of eukaryotic cells, may be an effective tool against HPV-induced cervical cancer, due to its preventive potential and therapeutic effects. To maximise the efficiency of these vaccines, the development of an appropriate delivery system is critical.

Thus, the present work was based on the optimization of the formulation of delivery systems based on the chitosan polymer, and four types of chitosan with different molecular weights were explored: high molecular weight chitosan (HMW, 200-500 kDa), low molecular weight (LMW, 50-190 kDa), 20 kDa and 5 kDa. The technique used to formulate the systems was the ionotropic gelation, based on ionic crosslinking. The nanoparticle formulation resulted from the interaction established between the positively charged chitosan polymers, and the negatively charged crosslinker sodium tripolyphosphate (TPP) and the plasmid DNA (pADN), encoding mutated E7. The inclusion of TPP aims to compact the formed nanoparticles and increase their stability, thus favouring a more defined round shape. To achieve the best delivery systems, a design of experiments (DoE) tool was used. This tool allowed combining several

parameters/inputs simultaneously (chitosan and TPP concentrations) to obtain the optimal formulation conditions of the systems based on the chosen responses (size, polydispersity index (PDI) and zeta potential). After performing the proposed tests and characterizing the properties of the obtained formulations, the respective responses were introduced in the DoE program and a statistical analysis was performed. The linear and quadratic models obtained were statistically significant (p-value <0,05) and the "lack of fit" was not significant, with an adequate determination coefficient. The predicted optimal points for each chitosan polymer were all successfully validated.

Subsequently, further studies were conducted to evaluate the properties of the delivery systems formulated with the conditions defined at the optimal points. Scanning electron microscopy (SEM) analyses were performed to evaluate the morphology, Fourier transform infrared spectroscopy was used to evaluate the chemical properties and specific functional groups, while different stability tests were performed to evaluate the strength and DNA release, and finally cytotoxicity tests were performed to ensure the biocompatibility of the chitosan nanoparticles. The four delivery systems developed, presented satisfactory characteristics, such as spherical or oval nanoparticles, good stability and strength, DNA retention and good biocompatibility.

In this sense, the DoE tool proved to be a powerful tool to explore and tailor the characteristics of chitosan/TPP/pADN nanosystems, allowing the development of a system suitable for the encapsulation, transport and delivery of pADN, thus providing the advancement of the DNA vaccine delivery research field.

Keywords

Chitosan polymers; delivery systems; design of experiments; DNA vaccine; HPV.

Index

Chapter 1 – Introduction.....	1
1.1. Cancer Overview	1
1.2. Cervical Cancer	2
1.3. HPV (Human papillomavirus)	3
1.4. HPV Genome	4
1.5. E6 and E7 oncoproteins	4
1.6. HPV – Current prevention methods.....	7
1.7. Cancer therapeutic-based DNA vaccines	8
1.8. Immune response induced by DNA vaccines	9
1.9. Gene delivery systems	10
1.9.1. Viral vectors	10
1.9.1.1. Retrovirus vectors	11
1.9.1.2. Adenovirus vectors.....	11
1.9.1.3. Adeno-associated virus (AAV) vectors	11
1.9.1.4. Lentivirus vectors	11
1.9.2. Non-Viral vectors	12
1.9.2.1. Physical methods	12
1.9.2.2. Chemical methods.....	13
1.9.2.2.1 Cationic lipids	14
1.9.2.2.2. Cationic polymers.....	14
1.10. Chitosan	15
1.11. Chitosan delivery systems	16
1.11.1. Formulation methods	16
1.11.1.1. Ionic crosslinking	16
1.11.1.2. Spray Drying	17
1.11.1.3. Solvent evaporation	17
1.11.1.4. Precipitation or Flocculation	17
1.11.1.5. Chitosan solution coating.....	17
1.12. Design of Experiments (DoE).....	17
Chapter 2 – Aim of the thesis.....	20
Chapter 3 – Materials and Methods	22
3.1. Materials	22

3.2 Methods	22
3.2.1. Plasmid DNA Amplification and Purification.....	22
3.2.2. Agarose Gel Electrophoresis	23
3.2.3. Preparation of Chitosan/TPP/pDNA Nanoparticles	23
3.2.4. Design of Experiments (DoE).....	23
3.2.5. Characterization of Chitosan/TPP/pDNA Nanoparticles.....	24
3.2.6. Fourier Transform Infrared Spectroscopy.....	24
3.2.7. Stability Assays	24
3.2.8. Cell Culture and <i>In Vitro</i> Transfection Studies	25
3.2.9. Cytotoxicity Assays.....	25
Chapter 4 – Results and Discussion	27
4.1. Development of the delivery system	27
4.1.1. Choose of DoE inputs	27
4.1.2. Model Application and Analysis.....	29
4.3. Properties of the chitosan nanoparticles.....	40
4.3.1. SEM	40
4.3.2. Fourier Transform Infrared Spectroscopy.....	42
4.3.3. Stability Assays.....	44
4.3.4. Cytotoxicity Assays.....	48
Chapter 5 – Conclusions and future perspectives	51
Chapter 6 – References.....	54
Chapter 7 – Annexes	62

List of figures

Chapter 1 - Introduction

Figure 1: Cancer incidences over the world.	2
Figure 2: HPV genome organization and gene activity.	4
Figure 3: HPV E6 oncoprotein forming the complex E6/E6AP/p53 responsible for the degradation of p53.	5
Figure 4: HPV E7 oncoprotein responsible for the degradation of pRb.	6
Figure 5: HPV E7 and E6 oncoproteins working together to promote the overgrowth of deregulated cells.	7
Figure 6: Different pathways of the immune response to DNA vaccines.	10
Figure 7: Non-viral delivery system pathway for DNA delivery.	13
Figure 8: Examples of cationic lipids and polymers utilized in non-viral vectors formation.	15

Chapter 4

Figure 9: Variation of the nanoparticles size in different concentrations of A(Chitosan) and B(TPP).	28
Figure 10: Nanoparticles images obtained by SEM. (A) nanoparticles of 5 kDa chitosan. (B) nanoparticles of 20 kDa chitosan. (C) nanoparticles of LMW chitosan. (D) nanoparticles of HMW chitosan.	41
Figure 11: FTIR spectra (absorbance versus wavenumbers) of pDNA, TPP, chitosan with different molecular weights (HMW, LMW, 20 kDa, 5 kDa) and chitosan/TPP/pDNA nanoparticles.	43
Figure 12: Stability assays of chitosan nanoparticles at 1 h, 1 day, 1 week and 1 month. (A) Chitosan nanoparticles size after storage at room temperature. (B) Chitosan nanoparticles size after storage at 4 °C. (C) Chitosan nanoparticles PDI after storage at	

room temperature. (D) Chitosan nanoparticles PDI after storage at 4 °C. (E) Chitosan nanoparticles zeta potential at room temperature. (F) Chitosan nanoparticles zeta potential at 4 °C.45

Figure 13: Analysis of nanoparticles' stability in cellular incomplete medium by agarose gel electrophoresis. Evaluation of nanoparticles stability in MEM- α incomplete medium (A) and in DMEM-F12 incomplete medium (B) at 37 °C. Evaluation of nanoparticles stability in MEM- α complete medium (C) and in DMEM-F12 complete medium (D) at 37 °C.47

Figure 14: Electrophoretic analysis of the nanoparticles after 1 h incubation with heparin.48

Figure 15: Cellular viability of JAWSII and human fibroblasts cells at 48 and 72 h after transfection with the different chitosan/TPP/pDNA systems and naked DNA.49

List of Tables

Chapter 1

Table 1: Properties of DNA vaccines.	9
---	---

Chapter 4

Table 2: Central composite design and response values for four chitosan polymers.	30
--	----

Table 3: Central composite design and response values for HMW chitosan.	31
--	----

Table 4: Central composite design and response values for LMW chitosan.	32
--	----

Table 5: Central composite design and response values for 20 kDa chitosan.	32
---	----

Table 6: Central composite design and response values for 5 kDa chitosan.	33
--	----

Table 7: Coded multiple regression equations for each output assessed in the chitosan nanosystems formulation.	35
---	----

Table 8: Statistical coefficients obtained by the DoE for all chitosan polymers.	36
---	----

Table 9: ANOVA p-values for central composite design for the formulation of chitosan nanosystems.	37
--	----

Table 10: Optimal points for the four chitosan polymers.	39
---	----

List of Abbreviations

AAV	Adeno-associated virus
Ad5	adenovirus serotype 5
APCs	antigen-presenting cells
CCF	Central Composite Face
DLS	Dynamic Light Scattering
DMEM-F12	Dulbecco's Modified Eagle's Medium with Ham's F-12 Nutrient Mixture
DNA	Deoxyribonucleic Acid
DoE	Design of experiments
E6AP	E6-associated protein
E7mut	mutated E7 gene
EDTA	Ethylenediamine tetra-acetic acid
FADD	Fas-associated death domain
FBS	Foetal bovine serum
FTIR	Fourier transform infrared spectroscopy
HIV	Human Immunodeficiency Virus
HMW	high molecular weight
HPV	Human Papillomavirus
HSV	herpes simplex virus
IFN- γ	interferon-gamma
IgG	Immunoglobulin G
IL	Interleukin
LB agar	Luria-Bertani agar medium or Lysogeny broth
LCR	long control region
LMW	low molecular weight
MEM- α	Minimum Essential Medium α
MHC	major histocompatibility complex
mRNA	Messenger RNA
OD _{600nm}	optic density at 600 nm
PBS	phosphate buffered saline

PDI	Polydispersity index
pDNA	plasmid DNA
PEI	poly(ethyleneimine)
PKB	protein kinase B
PLGA	Poly(lactic-co-Glycolic Acid)
pRb	Retinoblastoma protein
RNA	Ribonucleic Acid
SEM	Scanning electron microscopy
TAE	Tris-Acetate-EDTA
TAs	tumour antigen
TB	Terrific Broth
TNF- α	tumour necrosis factor-alpha
TNF R1	tumour necrosis factor receptor 1
TPP	tripolyphosphate
WHO	World health Organization

List of Scientific Publications

Rodolfo, C., Eusébio, D., Ventura, C., Nunes, R., Florindo, H. F., Costa, D., & Sousa, Â. (2021). *Design of Experiments to Achieve an Efficient Chitosan-Based DNA Vaccine Delivery System*. *Pharmaceutics*, 13(9), 1369.

Chapter 1 – Introduction

1.1. Cancer Overview

In modern times, cancer is the second cause of death worldwide, but in a near future may become the first one. With such an impact on the global population, it is important to have rapid, as well as efficient, screening and diagnosis methods, but also good prevention and treatment strategies (Mattiuzzi & Lippi, 2019; Torre et al., 2016). To understand such a threatful disease, it is necessary to know their origins. Cancer is a genetic and epigenetic disease. It is a genetic disease due to mutations in genes, sporadic or inherited, that are responsible to maintain control of the cell cycle, tissue homeostasis or regulate apoptosis. On the other hand, it is an epigenetic disease due to epigenome alterations and mutations in chromatin-remodelling enzymes. These alterations/mutations is the result of histone protein marks or aberrant DNA removal or attachment (Sadikovic et al., 2008; Tiffon, 2018).

According to world health organization (WHO), the estimated cancer incidence in countries of first world are higher than the third world countries, reaching in almost all of them a level of incidence above of 257.1 per 100 000 habitants (Figure 1A). People from first world countries are expose to more lifestyle risk factors, like excess body weight, tobacco, physical inactivity, and reproductive patterns. All these factors contribute to a rise of incidence in first world countries. However, the tendency can change in the future, first world countries whit knowledge of risk factors, improved treatment, screening, and early detection of cancers have managed to decrease the incidence of some cancers. On the other hand, third world countries start to adopt some of risk factors of first world countries, contributing to a rise of cancer incidence (Torre et al., 2016). The three most dominant cancer by country, in the world, are breast, prostate and cervix uteri cancer (Figure 1B). Cervix uteri or cervical cancer has more incidence in countries of Africa and South America and it is mostly caused by the human papillomavirus (HPV) (Kessler, 2017).

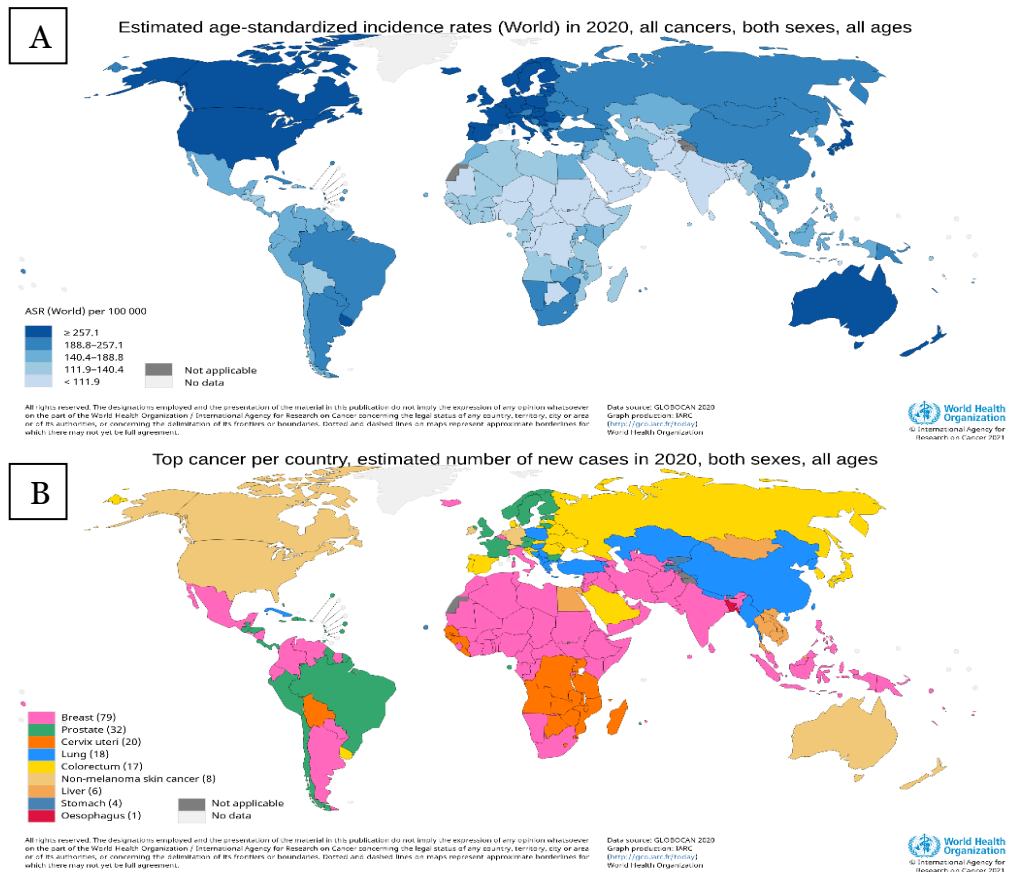


Figure 1: Cancer incidences over the world. (A) Map representing the incidence of all cancers in each country of the world. (B) Map representing the type of cancer with the higher incidence in each country of the world. (Adapted from(<https://gco.iarc.fr/>) accessed in 13/10/21).

1.2. Cervical Cancer

Cervical cancer is the fourth most common cancer in women all over the world and presents a big incidence in less developed countries, which contributing with 84% of the total number of cervical cancers. This difference can be related to the availability of vaccination against HPV and screening tests. In most developed countries, women are vaccinated in their teenage years, and prevention is controlled with resource to a Papanicolaou test, when precancerous lesions are found. Less developed countries struggle more with this cancer because they have to deal with societal barriers like illiteracy, poverty, spousal support, mistrust in healthcare system and antivaccination movement (Kessler, 2017; Vu et al., 2018).

The first years of a person with a persistent infection with HPV and progression to cervical cancer are often asymptomatic. However, when this disease present symptoms, the most common is irregular or heavy vaginal bleeding, mainly after sexual intercourse. Other types of symptoms include vaginal discharge, or in cases when the disease is more advanced, pelvic or lower back pain and bowel or bladder changes. Women who detect this cancer in early stages have almost 100% 5-year survival rate. Despite the survival rate of treatment, it is important to look upon the side effects at long-term, considering that a major part of the cases occur in women before age 49.

Some effects that might happen are bladder or bowel dysfunction loss of fertility and premature ovarian failure (Johnson et al., 2019; Kessler, 2017).

Some researchers believe that it will be possible to eradicate cervical cancer, but to achieve this goal, it is necessary to focus on vaccination and screening of the world's population (Canfell, 2019). Leaving open new possibilities for the development of new vaccines, or screening techniques or enhancing and improving existing ones.

1.3. HPV (Human papillomavirus)

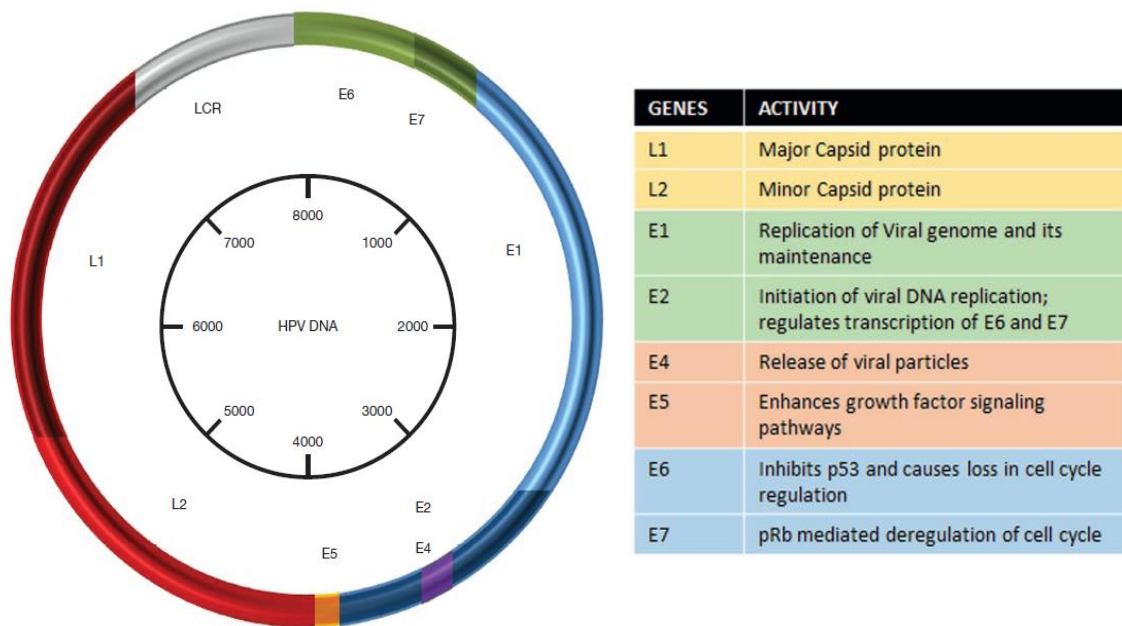
In 1983 was established a connection that cervical cancer is, in almost the totality of the cases, caused by HPV virus (Durst et al., 1983). This type of virus is transmitted by sexual contact, by infecting the genital areas of males and females. The HPV infection do not present symptoms, due to this particularity, the infected individuals are aware of the infection (Kessler, 2017). HPV is a virus belonging to the *Papillomaviridae* family. This virus is composed of a double-stranded DNA included in a group of non-enveloped double-stranded DNA viruses. Virus genetic material is kept in an icosahedral capsid, where the L1 and L2 proteins are the major and minor structural proteins (Pal & Kundu, 2020; Szymonowicz & Chen, 2020).

Although, HPV is associated at cervical cancer in most of the times, some researches link this virus to other cancers, such as vaginal, penile, vulval, anal and oropharynx. Today more than 200 types of HPV have been identified and characterized. These types can be divided into two categories: low-risk group and high-risk group, in consideration of the oncogenic potential of each virus (Adjei Boakye et al., 2017; Yang et al., 2016).

In the high-risk group are included the HPV16, 18, 31, 33, 35, 39, 45, 51, 52, 56, 58 and 59 types. All these types belong to a genus of HPV called mucosa alpha-papillomaviruses. From this group, HPV16 and HPV18 are the most predominant genotypes detected in cervical cancer cases, being responsible for 70% of the total cases (Hoppe-Seyler et al., 2018).

1.4. HPV Genome

HPV genome is constituted by 8 kb of DNA sequences and can be segmented into three parts (Figure 2). The first part is composed by the early gene-coding region (E), the second part contain the late gene-coding region (L) and the last part contain the long control region (LCR). E region encodes 7 different genes: E1, E2, E3, E4, E5, E6 and E7. E1 and E2 genes contribute to the transcription of early proteins and for the regulation of the viral genome, the other 4 genes are responsible to induce oncogenesis. Cancerous effect of HPV is mainly dependent on the production of E6 and E7 oncoproteins. These oncoproteins are acknowledged for interfere with the cell-cycle regulation and for affecting the signalling pathways to the cell apoptosis and repair. Whereas, the L region encodes 2 genes L1 and L2. The L1 code for the major viral capsid protein and the L2 code for the minor viral capsid structure. Finally, the LCR region does not have protein coding sequence, but contains the replication origin and numerous transcription factor binding sites for RNA polymerase II, making it easier to transcribe viral genome (Almeida et al., 2019; Pal & Kundu, 2020).



Genome organization of a high-risk Alphapapillomavirus
Expert Reviews in Molecular Medicine © 2017 Cambridge University Press

Figure 2: HPV genome organization and gene activity (adapted from (Pal & Kundu, 2020; Tsakogiannis et al., 2017)).

1.5. E6 and E7 oncoproteins

HPV E6 and E7 oncoproteins have an important key role in the development of oncogenic disease. During an HPV-positive cancer, host cells infected by this virus produce E6/E7 oncoproteins in an uncontrolled way. These oncoproteins have a length of approximately 150 and 100 amino acids and are known for contributing to the “hallmarks of cancer”, which constitute the six main alterations of cancer cells: resisting to cell death, enable replicative immortality, inducing

angiogenesis, activation of tissue invasion and metastasis, sustained proliferative signalling and evading growth suppressors. With these effects on the cells, these oncoproteins interfere with cell-cycle regulation, providing an inefficient signalling pathway for cell repair and apoptosis (Almeida et al., 2018, 2019; Derbie et al., 2020).

The HPV E6 oncoprotein is composed by 150-160 amino acids and originates, a protein with 18 kDa that has two zinc fingers formed by two pairs of CXXC motifs (Pal & Kundu, 2020). Its most important role is the interaction with p53 tumour suppressor, which will induce its degradation via ubiquitin. To target the p53 tumour suppressor, the E6 oncoprotein needs to bind to an E6-associated protein (E6AP) through an LXXL motif. Only after combination of E6/E6AP, the E6/E6AP/p53 complex is formed and proceeds to proteasomal degradation (Figure 3). Even though, the main anti-apoptotic process of this oncoprotein is the interaction with p53, the complex E6/E6AP also targets a protein called Bak. This protein is expressed in the upper epithelial layers and also has a cellular pro-apoptotic role. The Bak is also degraded by proteasome after binding with the complex E6/E6AP. Besides the interaction with these two proteins, E6 also targets other host apoptotic machinery, like the adaptor molecule Fas-associated death domain (FADD), procaspase 8 and tumour necrosis factor receptor 1 (TNF R1). HPV E6 oncoprotein also interacts with the cellular DNA replication machinery, through activation of telomerase, preventing the shortening of telomerases and thus allowing the continued cell proliferation (Hoppe-Seyler et al., 2018; Tomaić, 2016).



Figure 3: HPV E6 oncoprotein forming the complex E6/E6AP/p53 responsible for the degradation of p53 (adapted from (Sluimer & Distel, 2018)).

The HPV E7 oncoprotein is formed by 98 amino acids and has a C-terminal zinc-binding domain that is very important for E7 activity. This oncoprotein has three conserved domains designated CD1, CD2 and CD3. The CD1 and CD2 belong to short parts of conserved regions 1 and 2 from the Adenovirus E1a, and the CD3 is equivalent to SV40 large T antigen. A major part of the characterized functions of this oncoprotein has been linked to the CD2 and CD3 regions. However, it is important for the interactions between E7 oncoprotein and cellular substrates, that the protein maintains its overall integrity (Pal & Kundu, 2020; Tomaić, 2016).

CD1 domain of the E7 oncoprotein, is formed by the first 20 amino acids and has a very critical role inducing S-phase progression and cellular transformation. This domain binds the UBR4/p600, a protein fundamental for membrane morphogenesis, being considered a process very important for cell migration and necessary for cell survival (Tomaić, 2016).

Subsequently, the CD2 domain is formed by the amino acids 20 to 38. This domain contains the LXCXE binding motif and the CKII phosphorylation site, which is crucial for the binding into proteins like the retinoblastoma (pRb) tumour suppressor. The CKII phospho-acceptor site has a major role for the interaction with pocket proteins, one of the crucial characterized functions of E7. In cells infected with HPV, the LXCXE motif of the E7 oncoprotein target the unphosphorylated pRb for degradation through the ubiquitin proteasome pathway. With the degradation of pRb, the oncoprotein causes the disruption of the complex pRb-EF2, releasing free EF2. Due to these interactions, E7 oncoprotein has the critical effect of affecting the cell cycle progression, contributing for an environment suitable for DNA replication (Figure 4). Besides the pRb, the E7 also binds to proteins, such as p107 and p130, that have important roles in the regulation of cellular differentiation and apoptosis (Tomaić, 2016).

The C-terminal CD3 region is constituted by the amino acids 38-98. This region contains four highly conserved cysteine residues, responsible for the interaction with several cellular proteins, like p21 and p27 CDK inhibitors. Besides, E7 also contributes to the phosphorylation of p21 by inducing the protein kinase B (PKB), preventing its nuclear activities (Tomaić, 2016).

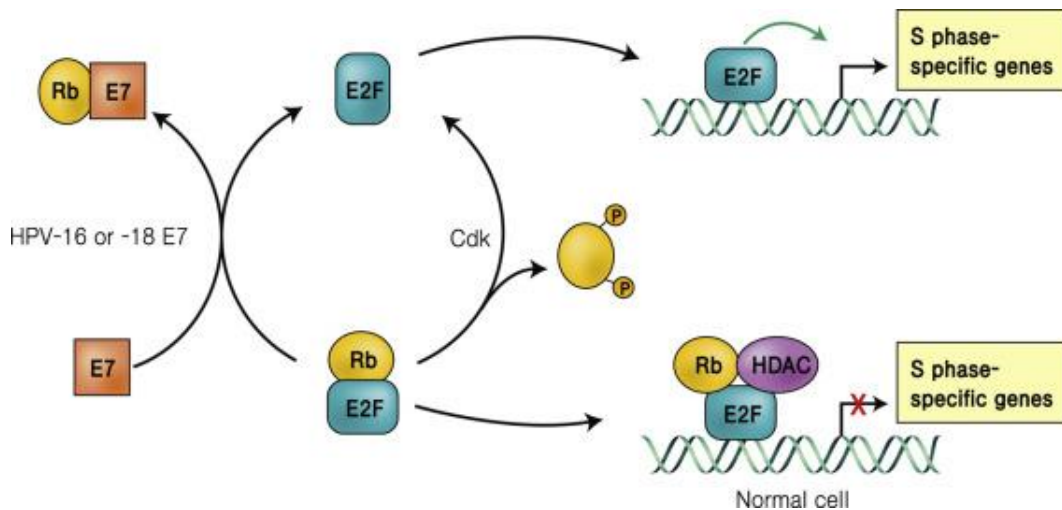


Figure 4: HPV E7 oncoprotein responsible for the degradation of pRb (adapted from (Trent, 2012)).

The HPV oncoproteins have a good performance together, since the increasing of E6 production the activity of E7 raises too. The combined targeting of various proteins by the E6/E7 lead to the growth of deregulated cells (Figure 5) (Hoppe-Seyler et al., 2018).

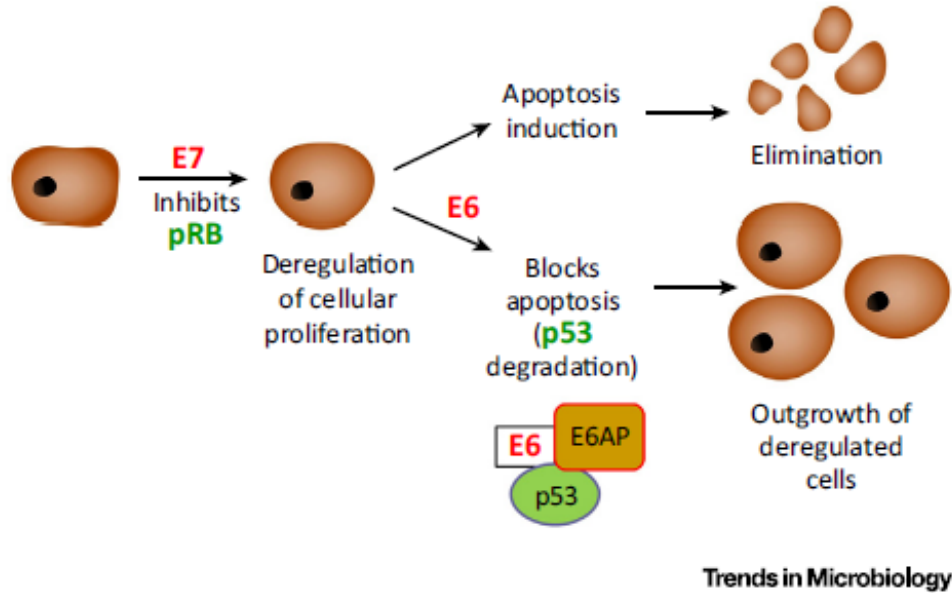


Figure 5: HPV E7 and E6 oncoproteins working together to promote the overgrowth of deregulated cells (adapted from (Hoppe-Seyler et al., 2018)).

1.6. HPV – Current prevention methods

Cervical cancer is a disease with high preventable rate, because of the effective screening and vaccination, already existing in developed countries, for the most carcinogenic HPV strains. For the proper prevention of this cancer, it is recommended to have a good education about risk factors, a complete vaccination series, and standardized screening (Hoppe-Seyler et al., 2018).

Screening women for cervical cancer or HPV infections is one of the prevention methods. The recommended age to start the screening is variable, depending on the country. Regardless of the start, screening tests are the Papanicolau cytology test with a sensitivity of 55.4% and the HPV co-testing (Hybrid Capture 2 test) with a sensitivity of 94.6%. Together, these two tests enable to evaluate the high-risk strains of HPV (El-Zein et al., 2016; Johnson et al., 2019; Mayrand MH et al., 2007).

Preventive vaccination is utilized in the fight against HPV infection. In current days, there exist three licensed HPV vaccines:

- Gardasil, a vaccine preventing against four different HPV strains, targeting the HPV 6, HPV11, HPV16 and HPV18;
- Cervarix, a vaccine preventing against two different HPV strains, targeting the HPV16 and HPV18;

- Gardasil 9, a vaccine preventing against nine different HPV strains, targeting the HPV6, HPV11, HPV16, HPV18, HPV31, HPV33, HPV45, HPV52 and HPV58.

The first HPV vaccine to be admitted was the Gardasil, approved in 2006 by the United States Food and Drug Administration. After a year, in 2007 the Cervarix vaccine was approved, and finally Gardasil 9 was approved in 2014. All these vaccines are based on virus-like particles (VLP), assembled from the recombinant expression of the L1 protein belonging to the HPV capsid. These VLP lack the oncogenic viral genome but remains morphologically identical to the native virions (Johnson et al., 2019; R. Wang et al., 2020).

However, as mentioned before, less developed countries have troubles and conflicts to apply these recommendations and in developed countries the prevention is not 100% effective. Existing vaccines are limited because they only provide a preventive immune response for future infections. If a person vaccinated already have an HPV infection, these vaccines have no therapeutic response. This limitation of current vaccines, opens the path to the development of therapeutic HPV vaccines with the aim of treating existent HPV infections but also prevent future HPV infections (R. Wang et al., 2020; Yang et al., 2016).

1.7. Cancer therapeutic-based DNA vaccines

In current times, there are many studies with good perspectives, aiming the development of therapeutic DNA vaccines for the cancer prevention and treatment (J. Wang et al., 2020). With the present pandemic induced by the coronavirus 2 (SARS-CoV-2) that the world is living, research on mRNA and DNA vaccines were reinforced and a major step has been taken with the approval of two mRNA vaccines against this virus. The first mRNA vaccine approved was BNT162b2 manufactured by Pfizer/BioNTech, and later, it was approved another mRNA vaccine manufactured by Moderna called mRNA-1273 vaccine (Moura et al., 2020; Ortega Rodríguez et al., 2021). These achievements are an important step for the study and understanding of the immune response of nucleic acid vaccines, but also to gain the trust of the worldwide population in these new methods of immunotherapy.

Therapeutic vaccination against cancer is a promising strategy, which aims to induce a specific and long-term immune response against a tumour antigen (TAs). Proteins overexpressed by the tumour tissue, that have an important impact on the tumour development and metastasis, are considered TAs. Along the years, some cancer vaccines have been developed by resorting to TAs obtention. Gene-based vaccines, such as DNA and mRNA vaccines, have the intention to induce these TAs expression in patient's antigen-presenting cells (APCs), thus helping to develop an immune system response against these agents (Lopes et al., 2019; J. Wang et al., 2020).

DNA vaccines are increasingly a promising option for a future strategy to combat cancer worldwide. Table 1 shows some properties of these type of vaccines. These vaccines are designed to deliver encoding genes (from TAs), aiming to improve the immune system response towards

the tumour cells that have the presence of the respective TAs. To date, no DNA vaccine against cancer has been approved for human use, but there are some DNA vaccines in study that reached clinical phases I, II or III (Lopes et al., 2019).

Table 1: Properties of DNA vaccines (adapted from (Lee et al., 2020)).

Vaccine type	Administration	Production	Biosafety	Storage and Transportation
DNA vaccines	Intramuscular, intradermal, subcutaneous and mucosal	Good molecular stability, low cost and good encapsulation	Do not live components, fewer side effects, poor autoimmune response, poor integration on genome and can induce indel mutations	Less need for cold chain delivery

1.8. Immune response induced by DNA vaccines

DNA vaccines have distinguished characteristics of conventional vaccines, such as the low-cost production, thermostability, easy distribution and promising immunological response at humoral and cellular level (Almeida et al., 2019).

These vaccines intend the DNA delivery, composed by genes or small gene fragments that encode immunogenic proteins, to host's cells. As route of administration, the intramuscular, intradermal, subcutaneous and mucosal pathways can be used, in order to achieve an efficient humoral and cell-mediated immune responses. The main targeting cells of these vaccines are APCs, and in less extension somatic cells, like myocytes (Lopes et al., 2019; Moura et al., 2020).

In figure 6, two pathways of the immune response are presented. These two pathways lead to different responses from the immune system because of the major histocompatibility complex (MHC), responsible for the antigen presenting to different lymphocytes. The cellular response starts with the activation of CD8 T cells by the antigen presentation through MHC class I complexes. Activated CD8 T cells stimulate the release of cytokines, such as tumour necrosis factor-alpha (TNF- α) or interferon-gamma (IFN- γ). By stimulating the release of cytokines, inhibits viral replication and MHC class I expression raises, causing the macrophages activation to support this cell-mediated immune response. Humoral response is triggered by the antigen presentation through MHC class II complexes, to CD4 helper T-cells. These CD4 helper T-cells are responsible for the activation of naïve B cells. After the activation, B cells will induce the production of different antibodies, mostly IgG classes to protect the host from the disease. APCs also contribute for the immunization process, by the liberation of chemokines and

proinflammatory cytokines, such as IL4, IL-10, IL-12 and TNF- α , involved in the activation process of T cells (Li & Petrovsky, 2016; Lopes et al., 2019; Moura et al., 2020).

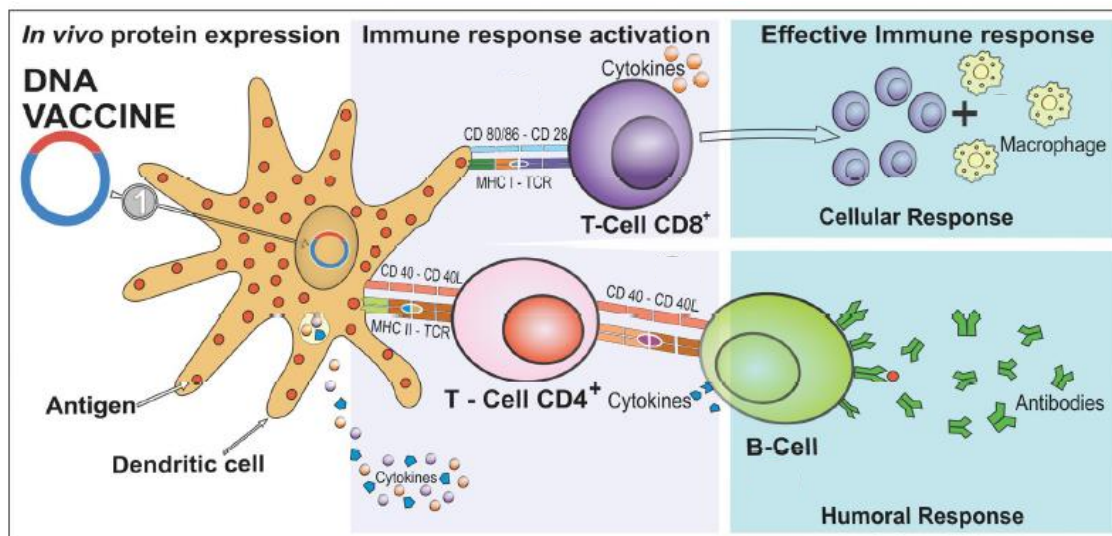


Figure 6: Different pathways of the immune response to DNA vaccines (adapted from (Moura et al., 2020)).

The naked DNA has poor transfection efficiency of eukaryotic cells due to the repulsion of negative charges of phosphate groups and eukaryotic membrane. To overcome this limitation and protect DNA from nucleases degradation, formulation of delivery systems is a promising solution.

1.9. Gene delivery systems

The delivery systems will help DNA, which encode the desired gene, to arrive to target host cells and overcome several extra- and intracellular barriers imposed by the immune system and target cells. The DNA vaccine must be protected from degradation induced by components of circulation and extracellular environment and find target cells. On the other hand, DNA vaccines should also cross the cellular membrane through pinocytosis or endocytosis, avoid degradation by lysosomes and endosomes, survive to cytosolic nucleases and penetrate the nuclear envelope. To help DNA overcoming these barriers several gene delivery systems has been studied, aiming DNA protection, carrier and suitable delivery. Delivery systems can be divided in two groups: viral vectors and non-viral vectors (Suschak et al., 2017).

1.9.1. Viral vectors

Viral vectors are formed by modified virus, like retrovirus, adenovirus, lentivirus, adeno-associated virus, between other, to carrier the DNA. To be used as delivery systems, these viruses must be modified through a process called transduction to replace viral genes, responsible to the virulence and virus replication, by heterologous genes. Viral vectors take advantage of virus capabilities regarding the reproduction, cell targeting and evasion, without the production of infectious virus. These delivery systems present several advantages, such as highly specific delivery of genes to target cells, great efficiency gene transduction and a strong immune response.

However, they have some drawbacks, such as immunogenicity, carcinogenesis, limitation of DNA packing capacity, broad tropism, and difficulty on vector production/manufacturing (Mali, 2013; Vannucci et al., 2013; Yin et al., 2014).

1.9.1.1. Retrovirus vectors

Retrovirus are virus enveloped with a capsid. Inside the capsid, there are two copies of single-stranded RNA with approximately 7-11 kbp. This vector can host 7-8 kbp of foreign DNA inserts. When the vector arrives to its destination cell in the host, it converts the RNA into double stranded DNA, using the reverse transcriptase process. Then, DNA is transported into the nucleus and eventually integrated in the cell genome. Retrovirus do not efficiently infect non-dividing cells (Mali, 2013; Ura et al., 2014; Yin et al., 2014).

1.9.1.2. Adenovirus vectors

Adenovirus are composed of a non-enveloped icosahedral capsid with a single double-stranded DNA. Approximately 50 human adenovirus serotypes have been identified, among them the most investigated is the human adenovirus serotype 5 (Ad5) due to easy production. This virus is utilized as vector due to its low pathogenicity, high expression level of viral proteins over replication, the viral genome delivery in the nucleus and infection properties. This type of vectors can infect dividing and non-dividing cells and can carry 8-10 kbp of foreign DNA (Ura et al., 2014; Vannucci et al., 2013).

1.9.1.3. Adeno-associated virus (AAV) vectors

Vectors like AAV are small and only carry 4.8 kbp of foreign DNA. They have a single-stranded DNA in a non-enveloped icosahedral capsid. The name of this virus is connected to the necessity of a helper virus to complete the replication cycle, which normally is the adenovirus. However, it is possible to use another virus as helper, such as herpes simplex virus (HSV). The AAV has low immunogenicity and do not show any pathogenicity. This vector integrates a specific region in the human genome at the chromosome 19q and remains silenced until the helper virus come to rescue him. The AAV can infect non-dividing and dividing cells (Mali, 2013; Ura et al., 2014; Vannucci et al., 2013).

1.9.1.4. Lentivirus vectors

Lentivirus is considered a subclass of retrovirus, but it is more complex. It can infect dividing and non-dividing cells unlike the retrovirus that only infect dividing cells. However, the capacity to carry foreign DNA remains almost the same, 9 kbp. The main difference is the presence of regulatory genes in lentivirus that have highly specific functions. A well-known virus is the Human Immunodeficiency Virus (HIV). This type of virus can originate good vectors due to the variety of target cells, some of them very difficult to transduce. Despite the low risk of triggering tumorigenesis, this is a limitation to the use of this virus as vectors (Ura et al., 2014; Vannucci et al., 2013).

1.9.2. Non-Viral vectors

Non-viral vectors emerged to answer the limitations of viral vectors, especially in terms of safety. In comparison with viral vectors, these vectors have a lower immunogenicity, can carry a much larger quantity of foreign DNA and are easily synthesized. The non-viral vectors consist of naked DNA/plasmid DNA, particle based or chemical based. To delivery these vectors to the host cells, physical and chemical methods can be explored. The most common used physical methods are needle injection, photoporation, sonoporation, gene gun, hydroporation and magnetofection. Chemical methods aim to offer DNA protection, for example by formulating small particles. These particles can be prepared by using natural or synthetic materials (Ramamoorth & Narvekar, 2015; Slivac et al., 2017; Sung & Kim, 2019; Yin et al., 2014).

1.9.2.1. Physical methods

The objective behind physical methods is to insert DNA into a target cell without resorting to a specific gene carrier. Through physical force, these methods force the membrane of the cell to make transient pores, allowing the passage of DNA into cells by diffusion. Advantages of these methods are safety, simplicity and control over the process parameters. As disadvantages are the low transfection efficiency and the need of a surgical intervention to delivery DNA to internal organs (Ramamoorth & Narvekar, 2015; Sharma et al., 2021).

One example of a physical method is the microneedles technique. This technique consists of the DNA injection directly into the targeted tissue by a set of small needles. DNA enters in the target cells by the damage and pressure caused by needle injection. It is a simple and easiest method, but also presents low efficiency due to quickly DNA degradation (Ramamoorth & Narvekar, 2015; Slivac et al., 2017).

Electroporation and photoporation are some of physical methods used. These two methods have the same principle, inducing pores in the cellular membrane to allow the DNA entry. In electroporation is used an electric field to form pores, while in the photoporation method, a single laser pulse is the responsible for the pore appearance. Both methods have good efficiency but can damaged cell membranes, causing the cell death (Ramamoorth & Narvekar, 2015; Sharma et al., 2021).

Gene gun is other example of physical methods. In this case, heavy metal particles are used, such as gold, silver, or tungsten, covered with DNA. This method uses the pressure of an inert gas or a high voltage electronic discharge to promote the crossing of particles through the membrane at a certain speed. Gene gun is reliable, simple, fast, have a good efficiency and have a precise delivery. However, this method is limited to superficial tissues, due to its shallow depth penetration (100-500 μm) and can cause tissue damages (Sharma et al., 2021; Slivac et al., 2017).

1.9.2.2. Chemical methods

As mentioned above, chemical methods normally apply cationic polymers, cationic lipids or polypeptides, to formulate small particles to carry drugs or nucleic acids. In the particular case of DNA, these particles grant its protection and also help in cell targeting or uptake (Sharma et al., 2021). Figure 7 shows an example of the pathway that these small particles must travel to deliver the DNA.

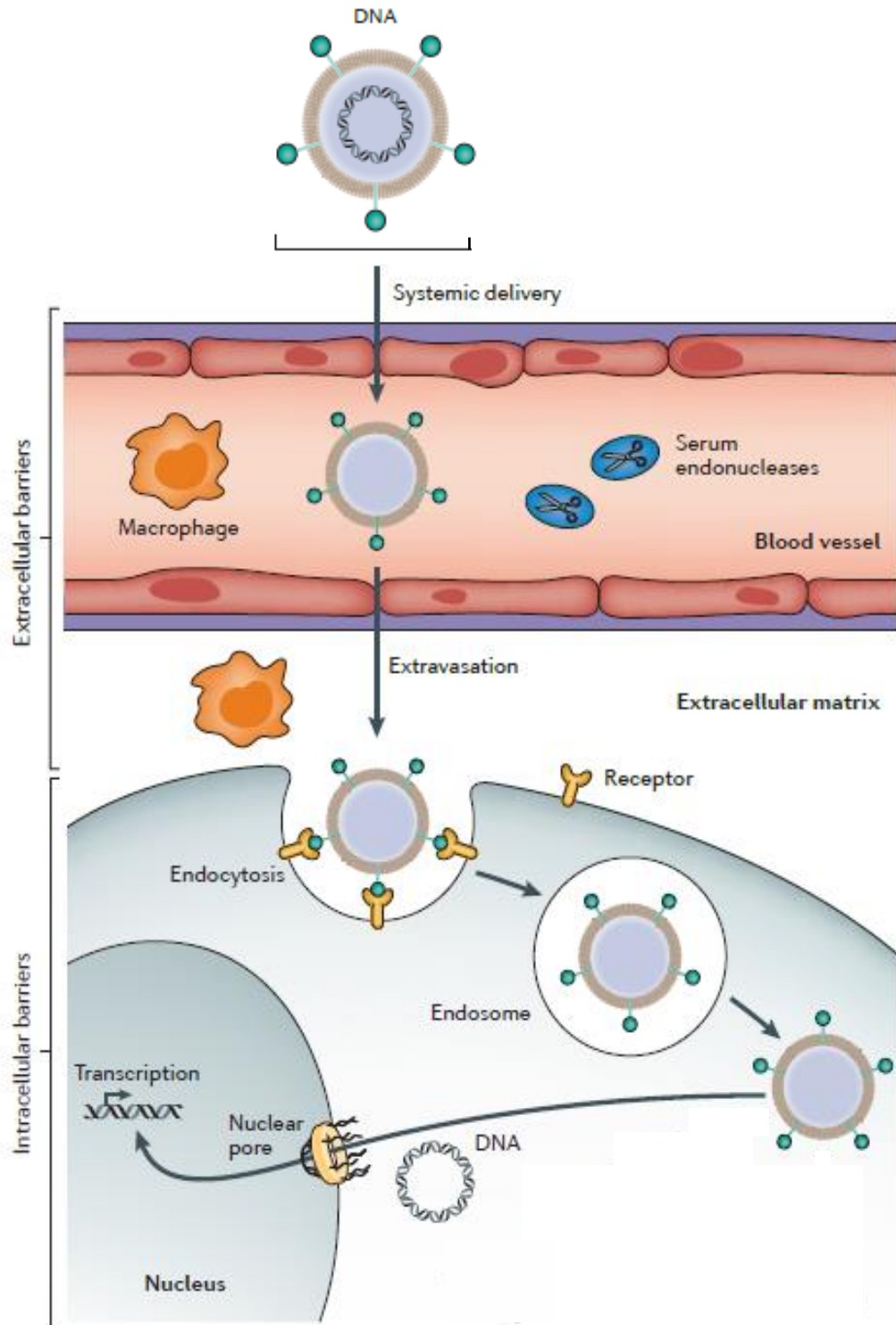


Figure 7: Non-viral delivery system pathway for DNA delivery (adapted from (Yin et al., 2014)).

1.9.2.2.1 Cationic lipids

One of the most non-viral vectors used as alternative to viral vectors is obtained with cationic lipids. There are many different cationic lipids in study (Figure 8a). Although, to form gene delivery complexes/nanoparticles, these cationic lipids must have three major characteristics: linker, polar headgroup and a hydrophobic tail. Polar headgroup is responsible for cationic binding to DNA. The binding occurs due to interaction between the positive headgroup and the negative phosphate groups of DNA. Hydrophobic tail is constituted by compounds of steroid structure and aliphatic chains. At last, the linkers between these two components are responsible to influence the transfection efficiency, biocompatibility, and stability of the lipid. When cationic lipids bind with DNA give rise to nanoparticles, also denominated lipoplexes. They confer protection to the DNA from the nuclease degradation and promote the cellular uptake. The nature of lipids, the lipids' structure and the lipid/DNA charge ratio are very important factors to the transfection efficiency of these lipoplexes (Ramamoorth & Narvekar, 2015; Sharma et al., 2021; Slivac et al., 2017).

1.9.2.2.2. Cationic polymers

Polymers positively charged are known as good non-viral vectors and many polymers remain in study (Shim et al., 2018). In comparison with cationic lipids, the positively charged cationic polymers bind with the negatively charged DNA, forming complexes called polyplexes. These complexes can be relatively smaller and are normally soluble in water, because they do not have any hydrophobic part. The polyplexes confer protection to the DNA against nucleases, help them to reach target cells and to overpass the cell membrane. The immune efficiency of cationic polymers depends on the polymer used, because each polymer confers certain characteristics to the polyplexes. As an example, chitosan can increase the immune efficiency due to the mucoadhesive characteristics (Mao et al., 2010). Currently, there are many available cationic polymers (natural or synthetic) used in the preparation of polyplexes, such as poly(ethyleneimine) (PEI), Polylactic-co-Glycolic Acid (PLGA), chitosan, and many others as showed in figure 8b (Sharma et al., 2021; Slivac et al., 2017; Yin et al., 2014) .

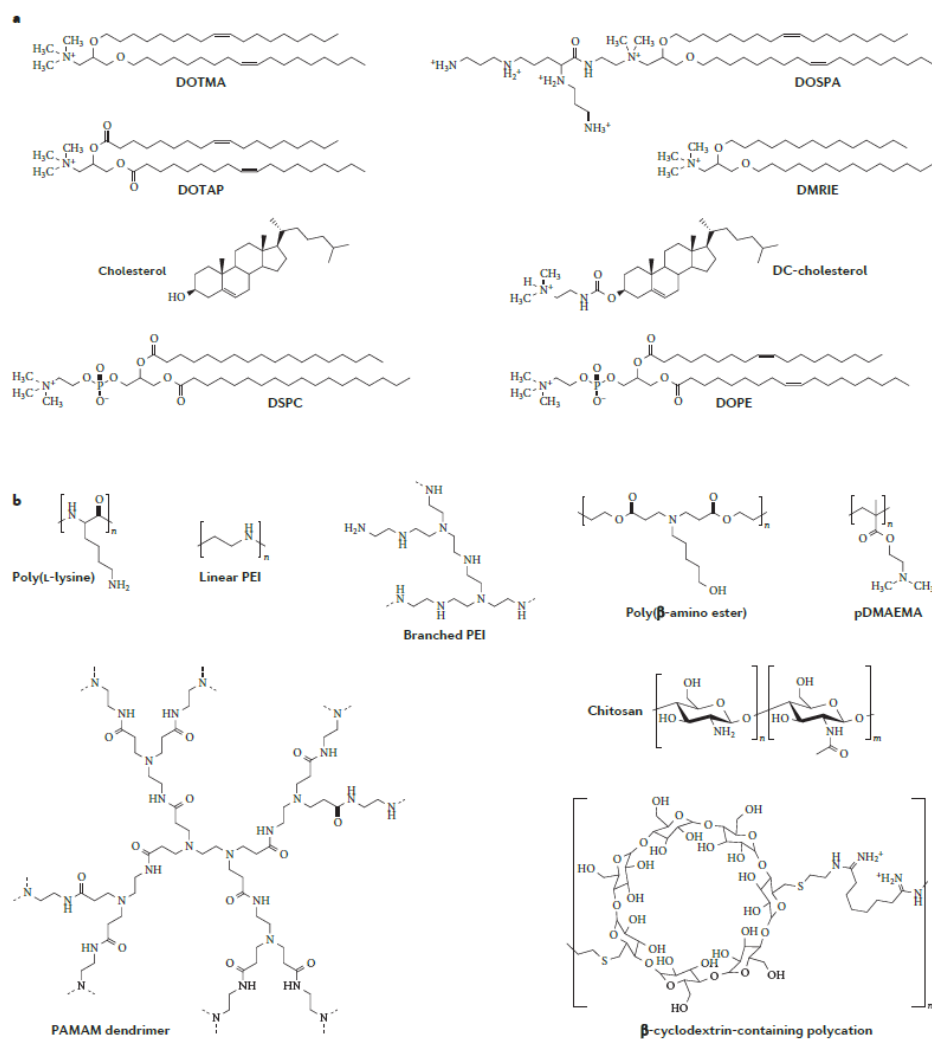


Figure 8: Examples of cationic lipids and polymers utilized in non-viral vectors formation. (a) Cationic lipids and (b) cationic polymers (adapted from (Yin et al., 2014)).

1.10. Chitosan

Chitosan is a cationic natural polymer, widely used in the nanoparticle's formulation for the delivery of drugs and nucleic acids. This polymer is obtained by deacetylation of chitin in an alkaline environment. As a biodegradable polysaccharide, chitin can be found in exoskeleton of crustaceans, cell walls of fungi and some plants. It is constituted by β -(1,4)-linked N-acetylglucosamine units, forming a linear homopolymer (Mao et al., 2010; D. Zhao et al., 2018).

Chitosan is considered a valuable polymer to be used in the formation of delivery systems because of its properties. One of the most important properties is the absence of toxicity since it does not show any immune response in the human body. This polymer also has antimicrobial activities, due to its positive charge. Thus, chitosan can interact with bacterial membranes and can interfere with fungal growth. In addition, this polymer shows high biocompatibility and biodegradability, being suitable to form delivery systems. Due to its structure and function resemblance to glycosaminoglycans, it presents a good biocompatibility and can be degraded by chitinases,

lysozyme and some colon bacteria. The mucoadhesive capacity of chitosan enables the adhesion into gastro-intestinal, upper respiratory tract and other mucous membranes, generating new approaches for delivery systems (Jhaveri et al., 2021; Rizeq et al., 2019; Surai, 2015; D. Zhao et al., 2018).

1.11. Chitosan delivery systems

In order to form chitosan nanoparticles or delivery systems, some factors like chitosan molecular weight, degree of acetylation, nucleic acids concentration, formulation method, between other, should be taken into consideration. Chitosan polymers can be presented in a specific or in range of molecular weight. Some studies showed that high molecular weight (HMW) chitosan tends to form bigger complexes than low molecular weight (LMW) chitosan (Bravo-Anaya et al., 2019). The acetylation degree of chitosan can affect the cellular uptake. Nanoparticles formed by high degree acetylated chitosan are more positive, facilitating the DNA binding and the cellular uptake. The nucleic acids concentration and the interaction between nitrogen groups of chitosan and phosphate groups of nucleic acids are also important factors in the formation of delivery system, because it may affect the size, charge and cellular uptake (Mao et al., 2010). If the balance between nitrogen groups and phosphate groups is not close to the optimal point, the created delivery systems have a tendency to an increased size (Gaspar et al., 2011). Cellular uptake and charge are related. The balance between the positively charged nitrogen groups and the negatively charged phosphate groups is important because, if there are more nitrogen groups the systems tend to be more positive and if there are more phosphate groups the system tend to be more negative (Mao et al., 2010; Turcsányi et al., 2020). The cell uptake increases with the increase of the positive charges (Yue et al., 2011; D. Zhao et al., 2018). However, to achieve a deliver system with specific characteristics, the used technique to create systems is one of the most important factors, because each technique has advantages and disadvantages. Some techniques can produce smaller nanoparticles, others produce nanoparticles with a better shape or positive zeta potential. Therefore, the technique must be chosen based on the desired characteristics for the delivery systems such as size, size uniformity, shape and zeta potential.

1.11.1. Formulation methods

Chitosan delivery system can be formed through a variety of methods, resulting into some changes between them. Each method has advantages and disadvantages. The most common methods used are ionically crosslinking, solvent evaporation, spray drying, precipitation or flocculation and chitosan solution coating (Sadeghi et al., 2008; D. Zhao et al., 2018).

1.11.1.1. Ionic crosslinking

The ionic crosslinking is the most common method utilized to form chitosan nanoparticles, which consists in the interaction between the positive charges from the chitosan and the negative charges from a crosslinker. There are many types of available crosslinkers, but tripolyphosphate (TPP) is the most used crosslinker. If the anionic crosslinker is added drop wise to the chitosan, while this is under stirring, the method is called ionotropic gelation (T. A. Ahmed & Aljaeid, 2016).

Ionotropic gelation has the advantage of being a simple process using water-based solutions and a very affordable method. However, this method can produce nanosystems with poor stability and wide particle size distribution, if not properly optimised (Fan et al., 2012; Jhaveri et al., 2021; Koukaras et al., 2012).

1.11.1.2. Spray Drying

In the spray drying technique, chitosan is dissolved in a solvent along with the inside content of the nanoparticle (can be drugs or nucleic acids), and it is optional to use a crosslinker. After the dissolution, components are sprayed into a drying chamber, which contains hot air that will evaporate the solvent and water, forming nanoparticles. Nanoparticles obtained with this method have spherical shape, an even size distribution and good stability. The use of hot air can be a disadvantage to the formulation of nucleic acid delivery systems (T. A. Ahmed & Aljaeid, 2016; Jhaveri et al., 2021; D. Zhao et al., 2018).

1.11.1.3. Solvent evaporation

In order to formulate nanoparticles with the solvent evaporation method, a solution prepared with chitosan and a surfactant is added to an organic solvent forming an emulsion. After a sonication, the solution stays under stirring conditions. While the solution is stirring, the organic solvent is evaporated, forming nanoparticles. Particles formed by this method present a spherical shape well defined and a smooth surface (Mohammed et al., 2017; D. Zhao et al., 2018).

1.11.1.4. Precipitation or Flocculation

To obtain delivery systems with this method, a precipitation or flocculation agent, like sodium sulphate, is added to the chitosan solution. A disadvantage of the method is that the obtained nanoparticles have a widely range of sizes (D. Zhao et al., 2018).

1.11.1.5. Chitosan solution coating

The chitosan solution coating technique consists in the addition of chitosan nanoparticles, already formulated, to another solution of chitosan. This process forms another layer of chitosan, providing a smooth surface to the nanoparticles, very good spherical shape, and a reasonable range of sizes. Nanoparticles formed by this technique present a controlled release of the content and have a good absorption (D. Zhao et al., 2018).

1.12. Design of Experiments (DoE)

Design of experiments (DoE) is an efficient analysis tool that can be used to optimize nanoparticles formulation, in a faster and easier manner, when compared with the common random experiment approach (Carlson, 2001; Myers et al., 2010; Valente et al., 2019). This tool allows the systematic and simultaneous variation of several parameters, applying a statistical model to use few experiments as possible (Canfell, 2019; Liu et al., 2017). This approach also considers the interaction effects between parameters, which sometimes is essential for better optimizing a process. Several models are available to apply in DoE. One of the models is the

Central Composite Face (CCF), which is composed of a full or fractional factorial design and start points placed on faces of sides. This model is useful to perform optimizations and can predict high-quality results, since it only uses points within the predetermined range. The application of DoE allows the faster advances of research, as well as a better time and cost management to researchers (Ben Ali et al., 2020; Székely et al., 2014).

Chapter 2 – Aim of the thesis

The aim of this thesis is to develop a chitosan delivery system to carry a pDNA encoding the E7 mutated protein, one of the main oncoproteins expressed during an HPV infection. The main idea is to create a nanocarrier with good properties, such as small size, positive charge, good stability, and biocompatibility, to be used in a therapeutic vaccine against cervical cancer in the future.

To achieve this objective, four chitosan polymers will be evaluated, applying formulation techniques based on ionic crosslinking. To formulate these systems, a DoE tool will be used, to reach the optimal point to obtain each delivery system. Thereafter, their properties will be analysed to ascertain the morphology, endurance, size, charge, and biocompatibility.

Chapter 3 – Materials and Methods

3.1. Materials

Medical grade high molecular weight (HMW) chitosan, with a molecular weight range between 200 and 500 kDa, was purchased from Heppe Medical (Halle, Germany). Low molecular weight (LMW) chitosan, with a molecular weight range between 50 and 190 kDa, chitosan of 5 kDa molecular weight and GRS Taq DNA polymerase were purchased from Sigma Aldrich Chemicals (St. Louis, MO, USA). Chitosan of 20 kDa molecular weight was purchased from Gletham Life Sciences (Corsham, UK). Sodium tripolyphosphate (TPP) was obtained from Across Organics (Geel, Belgium). TripleXtractor used in RNA extraction was obtained from GRISP (Porto, Portugal). Dulbecco's Modified Eagle's Medium with Ham's F-12 Nutrient Mixture (DMEM-F12) was purchased from GIBCO (Waltham, MA, USA). Minimum Essential Medium α (MEM- α) was purchased from HyClone classical media (Boston, MA, USA). Sodium bicarbonate was obtained from MP Biomedicals (Santa Ana, CA, USA). Agarose and GreenSafe was obtained from NZYtech (Lisbon, Portugal).

3.2 Methods

3.2.1. Plasmid DNA Amplification and Purification

The mutated E7 gene was cloned into pMC.CMV-MCS-EF1-GFP-SV40polyA parental plasmid cloning vector, next to CMV7 promoter, as described previously (Serra et al., 2021). Thus, the pDNA containing the mutated E7 gene (pDNA-E7mut) was amplified in ZYCY10P3S2T *Escherichia coli* host strain. Briefly, the host strain was inoculated in LB-agar petri dishes with kanamycin (50 mg/mL), and it was left overnight at 37°C. After this incubation phase in solid medium, some colonies were transferred to a 250 mL Erlenmeyer containing 62.5 mL of pre-fermentation liquid medium, Terrific Broth (20 g/L of tryptone; 24 g/L of yeast extract; 4 mL/L of glycerol; 0.017 M KH_2PO_4 , and 0.072 M K_2HPO_4 , pH 7.0). The Erlenmeyer was placed in the orbital shaker at 42°C and 250 rpm until the optic density at 600 nm ($\text{OD}_{600\text{nm}}$) reaches 2.6. At this moment, a certain volume of pre-fermentation medium was transferred to a 1 L Erlenmeyer containing 250 mL of Terrific Broth (TB) medium to start the fermentation with an $\text{OD}_{600\text{nm}}$ of 0.2. The Erlenmeyer was placed in the orbital shaker under previous conditions and left overnight (approximately for 12 h) until the bacterial growth reached the late log phase ($\text{OD}_{600\text{nm}} \sim 9$). Concluding this process, the bacterial growth was suspended by collecting the cells through centrifugation at 4500 *g* for 10 min at 4 °C, and the resultant pellets were stored at -2°C. Afterward, the pDNA-E7mut was purified by NZYMaxiprep kit (Nzytech, Lisbon, Portugal), according to the supplier's protocol.

3.2.2. Agarose Gel Electrophoresis

Along the work, all the agarose gel electrophoresis were prepared at 1% (w/v), by adding 1 g of agarose to 100 mL of 1× Tris-Acetate-EDTA (TAE) buffer (40 mM Tris base, 20 mM acetic acid, 1 mM Ethylenediamine tetra-acetic acid (EDTA) at pH 8.0) and stained with 1.2 µL of Green Safe from NZYTech (Lisbon, Portugal). Electrophoresis was carried-out for 40 min at 150 Volts and then the gels were imaged using ultraviolet (UV) light, by the Uvitec Fire-Reader system (UVITEC, UK).

3.2.3. Preparation of Chitosan/TPP/pDNA Nanoparticles

A stock solution (1 mg/mL) of each Chitosan polymer was prepared by resuspending the respective chitosan powder in sodium acetate buffer (0.1 M, pH 4.6), and a stock solution (1 mg/mL) of TPP was resuspended in the same buffer. In this work, four chitosan polymers were used with different molecular weights: namely the chitosan of HMW (200–500 kDa), LMW (50–190 kDa), 20 and 5 kDa. These solutions were stored at room temperature until use. The formulation of chitosan nanoparticles was performed by exploring the negatively charged TPP and the positively charged chitosan and the DoE tool. To determine the minimum and maximum level of each input to consider in the DoE, some preliminary studies were performed, exploring different techniques of nanoparticle formulation (complex coacervation and ionotropic gelation) and varying the chitosan and TPP concentrations between 0.1 and 1 mg/mL. The pDNA-E7mut was added to the TPP solutions to attain a final concentration of 20 µg/mL. Nanoparticles were formulated by adding, drop by drop, 100 µL of the TPP/pDNA solution to 400 µL of chitosan solution under vortexing for 1 min, with a volume ratio of chitosan and TPP + pDNA solutions of 4:1. Chitosan/TPP/pDNA-E7mut nanoparticles were left for 30 min at room temperature for stabilization, being subsequently centrifuged at 10,000 *g* for 10 min at 4°C.

3.2.4. Design of Experiments (DoE)

DoE was used to optimize the formulation of chitosan/TPP/pDNA nanoparticles of each chitosan polymer, minimizing the nanoparticles size, while maximizing the zeta potential and maintaining a suitable polydispersity index (PDI) (outputs). Two factors were considered as inputs, namely the chitosan and TPP concentration. These inputs were studied at three levels (-1; 0; +1), being the chitosan concentration input defined to 0.2, 0.5 and 0.8 mg/mL, while TPP concentration input defined to 0.25, 0.5 and 0.75 mg/mL, taking into account results from preliminary studies. Concerning the defined inputs and outputs, a CCF model was applied. Statistical analysis was performed, using Design-Expert version 11. The generalized second-order polynomial model equation used in the response surface analysis is presented below (Equation (1)):

$$Y = \beta_0 + \beta_1 X_1 + \beta_2 X_2 + \beta_{11} X_1^2 + \beta_{22} X_2^2 + \beta_{12} X_1 X_2 \quad (1)$$

After the analysis of the model suitability applied in DoEs, the optimal point to formulate nanoparticles with each chitosan polymer was determined and validated. The following studies were performed using input conditions determined in the optimal points.

3.2.5. Characterization of Chitosan/TPP/pDNA Nanoparticles

Nanoparticles were characterized to obtain the respective DoE outputs (size, potential zeta and PDI) and to determine their performance as DNA delivery systems. The average size, PDI and zeta potential measurements were achieved by Dynamic Light Scattering (DLS) at 25 °C using a Zetasizer Nano ZS equipment (Malvern Instruments, UK) and the Malvern Zetasizer software v6.34. Briefly, the average size and PDI were evaluated by mixing 500 µL of nanoparticles solution and 500 µL of ultrapure water and placed in a disposable cell. To evaluate the zeta potential, nanoparticles were centrifuged at 10,000× g for 10 min at 4°C and resuspended in MES buffer (0.01 M, pH 6,2). Each parameter was measured three times from three independent samples (n = 3), except the results of runs proposed by the DoE that are resultant from three measurements of each sample (n = 1). The DoE proposes to perform three runs (central points) under the same conditions (n = 3) to assess the model reproducibility.

Scanning electron microscopy (SEM) was used to evaluate the chitosan nanoparticles morphology obtained with optimal point conditions established by DoE to each polymer. Nanoparticles were centrifuged at 10,000× g for 10 min at 4°C, then resuspended in a phosphate buffered saline (PBS) solution for cleaning impurities. Once again, nanoparticles were centrifuged under previous conditions and resuspended in 40 µL of a solution containing tungsten. This solution was then placed in a round-shaped coverslip and dried overnight at room temperature. The dry samples were sputter-coated with gold using an EMitech K550 (London, UK) sputter coater. A Hitachi S-2700 (Tokyo, Japan) scanning electron microscope, with an accelerating voltage of 20 kV at various magnifications, was used.

3.2.6. Fourier Transform Infrared Spectroscopy

Fourier transform infrared spectroscopy (FTIR) was applied to evaluate the chemical structure of chitosan nanoparticles. The spectra were acquired using a Nicolet iS10 FTIR spectrophotometer (Thermo Scientific, Waltham, USA) with an average of 120 scans, a spectral width ranging from 4000 to 800 cm⁻¹ and a spectral resolution of 32 cm⁻¹. The spectra of isolated chitosan, pDNA and TPP samples were acquired for comparative analysis.

3.2.7. Stability Assays

Two different stability assays were performed with the formulated nanoparticles. The first assay aimed to assess the nanoparticle's colloidal stability over time, storing them in the formulation buffer and at different temperatures (Jonassen et al., 2012; Morris et al., 2011; Rázga et al., 2016). For that, nanoparticles were stored in sodium acetate buffer, at room temperature or 4°C. Nanoparticle characteristics, such as size, PDI and zeta potential, were evaluated throughout the

time at 1 h, 1 day, 1 week and 1 month. The statistical analysis was performed with two-way ANOVA followed by Tukey test (GraphPad Prism 9 software, GraphPad Software, San Diego, CA, USA). The second assay aimed to evaluate the nanoparticle's stability upon their incubation in the cell culture medium, with and without Foetal bovine serum (FBS) supplementation, to mimic the *in vitro* cell transfection conditions and extracellular environment of human body, to ensure the success of cellular transfection of these chitosan nanoparticles (Albuquerque et al., 2020; Serra et al., 2021). Thus, nanoparticles were centrifuged and resuspended in 50 μ L of DMEM-F12 or MEM alpha medium supplemented with 10% FBS or without this supplementation. Nanoparticles were further incubated at 37°C for 6 h and the pDNA release and degradation were monitored by 1% agarose gel electrophoresis. Decomplexation/degradation studies were performed to ensure that pDNA remained intact inside the delivery systems. For this study, nanoparticles were incubated at 60°C in the presence of heparin for 1 h and the pDNA release and degradation were monitored by 1% agarose gel electrophoresis (Strand et al., 2010).

3.2.8. Cell Culture and *In Vitro* Transfection Studies

The transfection studies were performed using human fibroblast cells (ATCC® PCS-201-012™) and murine immature dendritic JAWSII cells (ATCC® CRL-11904™). The human fibroblast cells were grown in DMEM/Ham's F-12 Nutrient Mixture (DMEM-F12) and JAWSII cells were grown in MEM α supplemented with GM-CSF (5 ng/mL). Both media were supplemented with 10% (v/v) FBS and 1% (v/v) of a mixture of penicillin (100 μ g/mL) and streptomycin (100 μ g/mL). Cells were incubated at 37°C in a humidified atmosphere containing 5% CO₂. Cells were seeded in a complete medium and 24 h before transfections, this medium was replaced by medium without supplements to promote transfection. Cells were transfected when 50–60% confluence was achieved, by adding to each well different nanoparticles resuspended in the medium without supplements. After 6 h of transfection, the medium was changed to fresh complete medium and cells were allowed to grow for different times, depending on the intended experiment.

3.2.9. Cytotoxicity Assays

To evaluate the nanoparticle's biocompatibility, a resazurin assay was used. This assay was applied in two different cell lines, human Fibroblast and JAWSII cells. Cells were seeded in 96-well plates with a density of 1×10^4 cells/well. Transfections with different chitosan systems and naked pDNA-E7mut were performed for 48 and 72 h. After, the culture medium was discarded and 100 μ L of fresh complete medium and 20 μ L of resazurin 0.1% (w/w) were added to each well. Cells were incubated in the dark over 4 h at 37°C in a humidified atmosphere containing 5% CO₂. Finally, the resorufin fluorescence was measured in a spectrofluorometer (SpectraMAX® Gemini™ EM, Molecular Devices, San Jose, CA, USA) by defining an excitation wavelength of 544 nm and an emission wavelength of 590 nm. Non-transfected cells were used as negative control and cells treated with 70% ethanol were used as the positive control. The statistical analysis was performed with two-way ANOVA followed by Tukey test (GraphPad Prism 9 software, GraphPad Software, San Diego, CA, USA).

Chapter 4 – Results and Discussion

4.1. Development of the delivery system

As previously mentioned, DNA vaccines are good tools to prevent and treat some cancers like cervical cancer. Aiming the design of a delivery system for carrying pDNA encoding for oncoprotein E7 mut, four different types of chitosan polymer were chosen, and a DoE tool was used to help with the design. This tool enabled the development and optimization of a delivery system with the targeted specifications. The development of nanocarriers by DoE started with the definition of the inputs of interest to meet the defined properties and therefore outputs. In order to choose the inputs of interest, background research and some preliminary tests were conducted to check which factors may have a major impact on the properties of these delivery systems. The second step involved the application of a DoE model and consequent analysis. The model utilized was the three-level CCF design. This model proposed 11 runs for each polymer and, after inserting the respective outputs, the DoE tool analysed the data of the runs and generated an optimal point for the delivery systems. After assessing the reproducibility of the optimal point for each formulation, the DoE was successfully applied.

4.1.1. Choose of DoE inputs

Chitosan has been widely used in the formulation of gene delivery systems. Several methods have been used to prepare chitosan delivery systems, and most of them consist of the interaction of positively charged chitosan and a negatively charged linker, such as DNA or TPP (Bravo-Anaya et al., 2019; de Pinho Neves et al., 2014; Deng et al., 2018; T. Huang et al., 2018; Köping-Höggård et al., 2004; Mao et al., 2010; Sadeghi et al., 2008; Q. Wang et al., 2017). In the beginning of this work, two methods were used for the preparation of the delivery systems: complex coacervation and ionotropic gelation. One of the most important factors for the formation of these complexes is the chitosan/TPP volume ratio. This factor affects the complex properties, like size, PDI, zeta potential and morphology. Considering previous studies, the chitosan/TPP volume ratio that resulted in complexes with good physicochemical properties was 4:1 (Deng et al., 2018; Gaspar et al., 2011; Sadeghi et al., 2008). Despite the chitosan/TPP volume ratio and concentration of respective solutions, other factors can affect the characteristics of these delivery systems, such as the molecular weight of chitosan polymers. Considering these key factors and aiming at an effective and efficient production of delivery systems, the influence of molecular weight was also evaluated in this work, optimizing by DoE the respective nanoformulations with the chitosan of HMW (200–500 kDa), LMW (50–190 kDa), 20 and 5 kDa.

To define the formulation technique and the input levels of the chitosan and TPP concentration, some preliminary studies were performed exploring the range of 0.1–1 mg/mL (Figure 9). The delivery systems prepared by the complex coacervation technique showed aggregation, while the ionotropic gelation technique led to delivery systems with acceptable characteristics. Figure 9 A represents the variation of the mean average diameter of the chitosan nanoparticles for different

concentrations of chitosan, while the concentration of TPP remains 0.5 mg/mL. On the other hand, figure 9 B represents the variation of nanoparticles' size for different TPP concentrations, while the chitosan remains at 0.75 mg/mL. The results show that for chitosan concentrations above 0.25 mg/mL, the size of the nanoparticles was lower than 200 nm. In addition, a portion of these carriers had positive charges and no aggregation was obtained for most of the concentrations tested, since the PDI was lower than 0.4, which indicates that the formulations present some homogeneity (Delan et al., 2020). Given this behaviour, ionotropic gelation was the selected formulation technique to proceed the work and input levels were defined to 0.2–0.8 mg/mL for chitosan polymers concentration and to 0.25–0.75 mg/mL for TPP concentrations. The chitosan/TPP volume ratio and pDNA concentration were kept constant along the study, being 4:1 and 20 µg/mL, respectively.

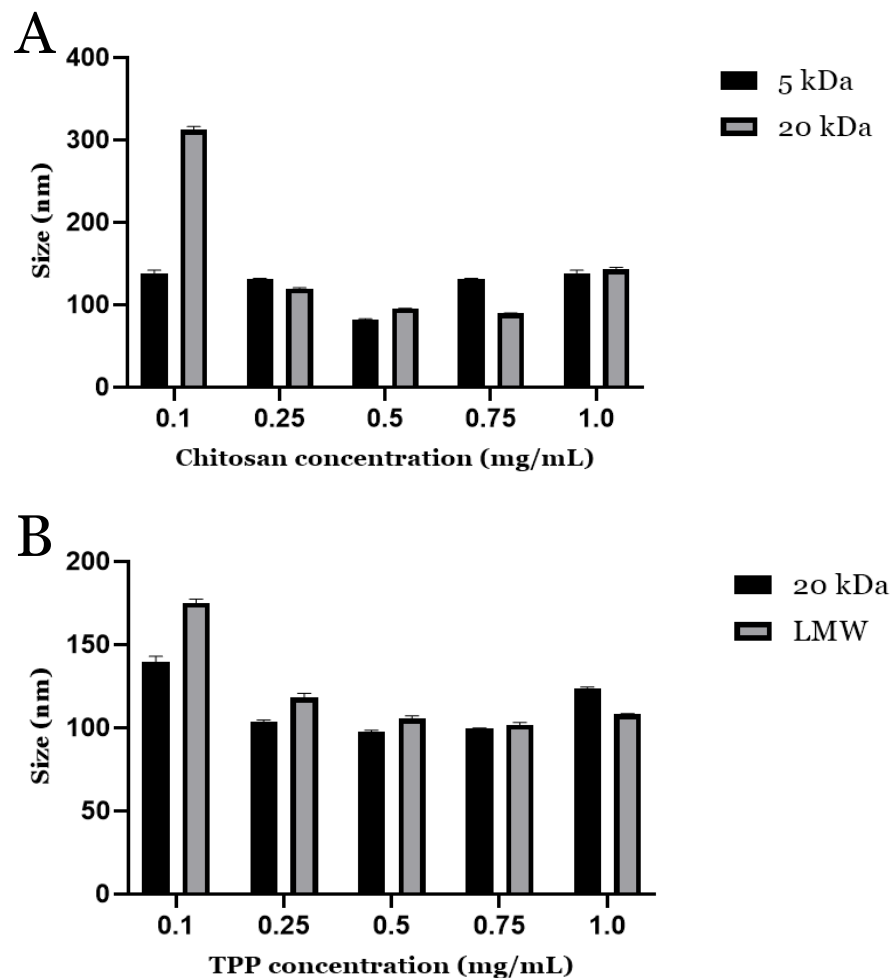


Figure 9: Variation of nanoparticles size using different concentrations of cationic and anionic formulation components. (A) Variation of chitosan concentration between 0.1-1.0, while TPP concentration remains at 0.5 mg/mL. Nanoparticles formulated with 5 and 20 kDa chitosans. (B) Variation of TPP concentration between 0.1-1.0, while chitosan concentration remains at 0.75 mg/mL. Nanoparticles formulated with LMW and 20 kDa chitosans.

4.1.2. Model Application and Analysis

After defining the DoE inputs, a three-level CCF design was applied to achieve the optimal nanoparticle formulation. This particular design is adequate for the present work because it does not consider points outside of the ranges established for the inputs (Ben Ali et al., 2020). Considering the results attained in preliminary studies, unsatisfactory results were expected using inputs outside the ranges, such as particle aggregation. In addition, the CCF model also allows the reduction of the number of experiments required to identify the optimal nanoparticles' formulation. In Table 2, all runs proposed by the DoE tool are presented for the four chitosan polymers, showing the concentrations used on nanoparticles formulation and the respective outputs. The model reproducibility was evaluated considering three central points ($n = 3$) to be performed under the same conditions, marked in grey in Table 2. The zeta potential, size and PDI outputs were determined by DLS. To avoid results inconsistency, all data shown in Table 2 represent the mean of three measurements for each output (run).

Table 2: Central composite design and response values for four chitosan polymers. (n = 3 ± SD)

Chitosan polymers	Chitosan Concentration (mg/mL)	Tpp Concentration (mg/mL)	Size (nm)	PDI	Zeta Potential (mV)
HMW Chitosan	0.20	0.25	115.0 ± 0.68	0.280 ± 0.002	20.57 ± 5.5
	0.20	0.50	210 ± 12.1	0.250 ± 0.050	14.4 ± 0.9
	0.20	0.75	249 ± 13.7	0.220 ± 0.080	9.82 ± 0.9
	0.50	0.25	125.0 ± 0.013	0.210 ± 0.013	29.5 ± 3.6
	0.50	0.50	156.0 ± 0.37	0.220 ± 0.050	25.6 ± 0.5
	0.50	0.50	158.0 ± 1.56	0.200 ± 0.013	27.1 ± 0.4
	0.50	0.50	167.0 ± 0.90	0.210 ± 0.015	25.6 ± 1.1
	0.50	0.75	180.0 ± 1.32	0.200 ± 0.011	26.9 ± 0.75
	0.80	0.25	133.0 ± 1.39	0.330 ± 0.050	30.3 ± 1.3
	0.80	0.50	172.0 ± 1.96	0.310 ± 0.008	32.0 ± 6.07
LMW Chitosan	0.20	0.25	109.0 ± 6.72	0.317 ± 0.017	20.3 ± 0.1
	0.20	0.50	88.05 ± 1.61	0.237 ± 0.006	14.4 ± 0.2
	0.20	0.75	85.11 ± 0.85	0.282 ± 0.013	9.82 ± 0.9
	0.50	0.25	106.6 ± 1.64	0.384 ± 0.052	20.9 ± 0.8
	0.50	0.50	94.41 ± 0.25	0.246 ± 0.004	15.1 ± 0.5
	0.50	0.50	98.00 ± 0.86	0.265 ± 0.016	15.9 ± 0.5
	0.50	0.50	96.39 ± 2.06	0.274 ± 0.009	15.9 ± 0.3
	0.50	0.75	96.81 ± 1.36	0.228 ± 0.001	13.6 ± 0.3
	0.80	0.25	128.1 ± 3.88	0.450 ± 0.028	27.0 ± 0.9
	0.80	0.50	114.1 ± 0.46	0.289 ± 0.010	24.0 ± 0.1
20 kDa Chitosan	0.20	0.25	141.5 ± 8.49	0.324 ± 0.008	17.5 ± 0.4
	0.20	0.50	121.0 ± 6.13	0.305 ± 0.027	15.8 ± 0.9
	0.20	0.75	116.0 ± 3.77	0.290 ± 0.022	10.1 ± 0.4
	0.50	0.25	110.8 ± 2.43	0.340 ± 0.011	20.7 ± 0.7
	0.50	0.50	106.1 ± 2.47	0.336 ± 0.030	17.1 ± 0.5
	0.50	0.50	102.0 ± 1.70	0.267 ± 0.018	18.9 ± 0.2
	0.50	0.50	102.6 ± 0.65	0.359 ± 0.017	18.1 ± 1.1
	0.50	0.75	86.15 ± 1.32	0.201 ± 0.003	14.1 ± 0.2
	0.80	0.25	107.0 ± 2.49	0.331 ± 0.012	21.9 ± 0.6
	0.80	0.50	97.95 ± 2.89	0.250 ± 0.015	19.6 ± 0.6
5 kDa Chitosan	0.20	0.25	83.05 ± 0.51	0.256 ± 0.002	19.1 ± 1.1
	0.20	0.50	84.41 ± 0.39	0.209 ± 0.008	17.5 ± 0.8
	0.20	0.75	109.1 ± 1.45	0.159 ± 0.009	13.0 ± 1.0
	0.50	0.25	91.28 ± 0.44	0.262 ± 0.006	21.8 ± 0.5
	0.50	0.50	77.68 ± 0.19	0.217 ± 0.005	18.7 ± 0.5
	0.50	0.50	77.91 ± 0.23	0.235 ± 0.006	17.5 ± 0.8
	0.50	0.50	74.82 ± 0.70	0.196 ± 0.009	18.4 ± 0.5
	0.50	0.75	80.11 ± 1.34	0.186 ± 0.005	15.2 ± 0.5
	0.80	0.25	110.4 ± 1.94	0.365 ± 0.005	23.7 ± 1.2
	0.80	0.50	90.83 ± 2.09	0.240 ± 0.002	23.2 ± 0.7
0.80	0.75	82.21 ± 1.50	0.215 ± 0.003	18.6 ± 0.2	

Analysing individually the chitosan polymers, HMW chitosan originated nanoparticles with an average size between 115-216 nm, a PDI between 0.200-0.330 and a zeta potential between 9.82-32.0 mV. Through the results presented in Table 3, it was observed an increase on the nanoparticles size when the chitosan concentration increased for a constant TPP concentration of 0.20 mg/mL. However, this behaviour changes for higher TPP concentrations. The explanation for this behaviour, is due to the high concentrations of TPP that can provide more links with chitosan, forming larger nanoparticles (Gaspar et al., 2011; Pan et al., 2020). Zeta potential increased when the concentration of chitosan was raised and TPP concentration remained the same. In contrast, when the concentration of TPP was raised and chitosan concentration remained the same, the zeta potential decreased. This behaviour was related to the global charges resultant in each situation (Turcsányi et al., 2020). Lastly, PDI values decreased when TPP concentrations were raised. In order to identify the best concentrations, it was necessary to achieve the smallest size and PDI with a reasonable zeta potential. The positive zeta potential was a very important factor because it influences the internalization of nanoparticles by the cells (Yue et al., 2011; F. Zhao et al., 2011).

Chitosan polymers	Chitosan Concentration (mg/mL)	Tpp Concentration (mg/mL)	Size (nm)	PDI	Zeta Potential (mV)
HMW Chitosan	0.20	0.25	115.0 ± 0.68	0.280 ± 0.002	20.57 ± 5.5
	0.20	0.50	210 ± 12.1	0.250 ± 0.050	14.4 ± 0.9
	0.20	0.75	249 ± 13.7	0.220 ± 0.080	9.82 ± 0.9
	0.50	0.25	125.0 ± 0.013	0.210 ± 0.013	29.5 ± 3.6
	0.50	0.50	156.0 ± 0.37	0.220 ± 0.050	25.6 ± 0.5
	0.50	0.50	158.0 ± 1.56	0.200 ± 0.013	27.1 ± 0.4
	0.50	0.50	167.0 ± 0.90	0.210 ± 0.015	25.6 ± 1.1
	0.50	0.75	180.0 ± 1.32	0.200 ± 0.011	26.9 ± 0.75
	0.80	0.25	133.0 ± 1.39	0.330 ± 0.050	30.3 ± 1.3
	0.80	0.50	172.0 ± 1.96	0.310 ± 0.008	32.0 ± 6.07
	0.80	0.75	216.0 ± 11.3	0.270 ± 0.016	28.0 ± 0.75

Table 3: Central composite design and output values for HMW chitosan. (n =3 ± SD)

The LMW chitosan led to nanoparticles with an average size of 85.11- 128.1 nm, a PDI between 0.237-0.450 and a zeta potential between 9.82-27.00 mv. Table 4 shows that the formulation presenting the lowest particle size, also presented low PDI and the lowest zeta potential. Nanocarriers originated using the LMW chitosan presented higher diameters for increased concentrations of chitosan and TPP. The zeta potential trend was similar to the one presented by nanoparticles prepared using HMW chitosan, as it decreased for higher TPP or chitosan concentrations. Looking at the PDI results, it can be concluded that when TPP concentration increased, the PDI values decreased.

Table 4: Central composite design and output values for LMW chitosan. (n =3 ± SD)

Chitosan polymers	Chitosan Concentration (mg/mL)	Tpp Concentration (mg/mL)	Size (nm)	PDI	Zeta Potential (mV)
LMW Chitosan	0.20	0.25	109.0 ± 6.72	0.317 ± 0.017	20.3 ± 0.1
	0.20	0.50	88.05 ± 1.61	0.237 ± 0.006	14.4 ± 0.2
	0.20	0.75	85.11 ± 0.85	0.282 ± 0.013	9.82 ± 0.9
	0.50	0.25	106.6 ± 1.64	0.384 ± 0.052	20.9 ± 0.8
	0.50	0.50	94.41 ± 0.25	0.246 ± 0.004	15.1 ± 0.5
	0.50	0.50	98.00 ± 0.86	0.265 ± 0.016	15.9 ± 0.5
	0.50	0.50	96.39 ± 2.06	0.274 ± 0.009	15.9 ± 0.3
	0.50	0.75	96.81 ± 1.36	0.228 ± 0.001	13.6 ± 0.3
	0.80	0.25	128.1 ± 3.88	0.450 ± 0.028	27.0 ± 0.9
	0.80	0.50	114.1 ± 0.46	0.289 ± 0.010	24.0 ± 0.1
	0.80	0.75	108.0 ± 4.24	0.294 ± 0.028	21.6 ± 0.3

Nanoparticles prepared using 20 kDa chitosan presented a size range of 86.15-141.5 nm, a PDI range of 0.177-0.359 and a zeta potential range of 10.1-21.9 mv. Table 5 shows the results for runs performed using 20 kDa chitosan for nanoparticle formulation. These carriers presented lower mean sizes for higher chitosan or TPP concentrations. The zeta potential and PDI were similar to the ones presented by nanoparticles composed by LMW chitosan. The PDI decreased when higher TPP concentrations were used, while the zeta potential increased for higher concentrations of chitosan and lower TPP concentrations.

Table 5: Central composite design and output values for 20 kDa chitosan. (n =3 ± SD)

Chitosan polymers	Chitosan Concentration (mg/mL)	Tpp Concentration (mg/mL)	Size (nm)	PDI	Zeta Potential (mV)
20 kDa Chitosan	0.20	0.25	141.5 ± 8.49	0.324 ± 0.008	17.5 ± 0.4
	0.20	0.50	121.0 ± 6.13	0.305 ± 0.027	15.8 ± 0.9
	0.20	0.75	116.0 ± 3.77	0.290 ± 0.022	10.1 ± 0.4
	0.50	0.25	110.8 ± 2.43	0.340 ± 0.011	20.7 ± 0.7
	0.50	0.50	106.1 ± 2.47	0.336 ± 0.030	17.1 ± 0.5
	0.50	0.50	102.0 ± 1.70	0.267 ± 0.018	18.9 ± 0.2
	0.50	0.50	102.6 ± 0.65	0.359 ± 0.017	18.1 ± 1.1
	0.50	0.75	86.15 ± 1.32	0.201 ± 0.003	14.1 ± 0.2
	0.80	0.25	107.0 ± 2.49	0.331 ± 0.012	21.9 ± 0.6
	0.80	0.50	97.95 ± 2.89	0.250 ± 0.015	19.6 ± 0.6
	0.80	0.75	92.54 ± 0.97	0.177 ± 0.010	17.0 ± 0.2

Finally, 5 kDa chitosan-created nanoparticles presented a size range of 74.82-110.4 nm, a PDI between 0.159-0.365 and a zeta potential range of 13.0-23.7 mv (Table 6). Nanoparticles formulated with 5 kDa chitosan, displayed higher average diameters for higher TPP concentrations, when the cationic polymer was used 0.2 mg/mL. For 0.5 and 0.8 mg/mL concentrations of chitosan, once higher TPP concentrations were used, nanoparticles presented lower diameters. This behaviour for 0.2 mg/mL chitosan concentration, can be explained through the molecular weight of this polymer. Chitosans with low molecular weight have fewer β -(1,4)-linked N-acetyl-glucosamine units, consequently fewer positive charges compared to the the same concentration of a high molecular weight chitosan (Mao et al., 2010). With fewer positive charges to perform the bond between chitosan and TPP, the equilibrium between both compounds is affected and can be responsible for the increase on nanoparticle size (Gaspar et al., 2011). However, the PDI and zeta potential behaviour remains the same as the other chitosan polymers.

Table 6: Central composite design and output values for 5 kDa chitosan. (n =3 \pm SD)

Chitosan polymers	Chitosan Concentration (mg/mL)	Tpp Concentration (mg/mL)	Size (nm)	PDI	Zeta Potential (mV)
5 kDa Chitosan	0.20	0.25	83.05 \pm 0.51	0.256 \pm 0.002	19.1 \pm 1.1
	0.20	0.50	84.41 \pm 0.39	0.209 \pm 0.008	17.5 \pm 0.8
	0.20	0.75	109.1 \pm 1.45	0.159 \pm 0.009	13.0 \pm 1.0
	0.50	0.25	91.28 \pm 0.44	0.262 \pm 0.006	21.8 \pm 0.5
	0.50	0.50	77.68 \pm 0.19	0.217 \pm 0.005	18.7 \pm 0.5
	0.50	0.50	77.91 \pm 0.23	0.235 \pm 0.006	17.5 \pm 0.8
	0.50	0.50	74.82 \pm 0.70	0.196 \pm 0.009	18.4 \pm 0.5
	0.50	0.75	80.11 \pm 1.34	0.186 \pm 0.005	15.2 \pm 0.5
	0.80	0.25	110.4 \pm 1.94	0.365 \pm 0.005	23.7 \pm 1.2
	0.80	0.50	90.83 \pm 2.09	0.240 \pm 0.002	23.2 \pm 0.7
	0.80	0.75	82.21 \pm 1.50	0.215 \pm 0.003	18.6 \pm 0.2

In general, data demonstrate that all experiments allowed to formulate nanoparticles with some variations of physicochemical properties. The size and zeta potential of chitosan nanoparticles were mainly dependent on the molecular weight of the polymer used and, in less extension, the concentration of the polymer and TPP crosslinker considered. In this way, the size of chitosan nanoparticles decreased when the molecular weight of chitosan polymers was lower, whereby the HMW chitosan led to the highest particle size of 249 nm, while the 5 kDa chitosan allowed the production of particles with the lowest size of 74.82 nm. According to some studies, this behaviour in the chitosan nanoparticles' size can be explained by the increase on the viscosity and the decrease on the solubility obtained when a HMW polymer is used (Bruinsmann et al., 2019; MacLaughlin et al., 1998). For instance, when the molecular weight increases, the size and zeta potential of delivery systems also increases. Some works describe that HMW chitosan polymers can be more stable than LMW chitosan polymers, while LMW chitosan can release the DNA at higher extent than the HMW chitosan, which can be useful for gene expression once the

nanosystems are inside the cells (MacLaughlin et al., 1998; Mao et al., 2010). The chitosan concentration differently affects nanoparticles size in the four used polymers (Table 2). The HMW and LMW chitosan polymers formulate small nanoparticles when chitosan concentration is low. The 5 and 20 kDa chitosan polymers led to small nanoparticle sizes for intermediate and high concentrations, respectively. These results suggest that chitosan polymer concentration may depend on the molecular weight of the used polymer, since polymers with lower MW require higher concentrations to get the same crosslinking density with the TPP/pDNA than chitosan polymers with higher MW (Fan et al., 2012). Looking at Table 2, the influence of TPP concentration on nanoparticles size is also variable in function of different chitosan polymers. For the HMW chitosan, the nanoparticles size is smaller when TPP concentration is low. The LMW and 20 kDa chitosan nanoparticles presented lower mean diameters when higher TPP concentrations were used in the formulations. As already observed before, nanoparticle size is dependent on a strong relation between the molecular size and concentration of chitosan and the contribution offered by TPP concentration to the pDNA solution. The lower the molecular weight of the polymer used, the greater amount of this polymer and TPP will be needed to establish crosslinking with all chitosan chains present in solution (Gaspar et al., 2011).

On the other hand, zeta potential output increased with the increase of molecular weight and the concentration of chitosan polymer since the presence of positive charges also increases (de Pinho Neves et al., 2014). With TPP concentration increase, the zeta potential of nanoparticles decreased in all polymers. This behaviour was expected because TPP increased the negative charge of solution. In general, the PDI output was below 0.4, which indicates that the formulations present some homogeneity (Delan et al., 2020). Its variation was inconstant for the different polymers, although it was possible to verify a downward trend when the concentrations of TPP increased and the chitosan concentration remained constant. This slight decrease on the nanoparticles' PDI can be justified by the ionotropic gelation technique used, which consists of adding TPP/pDNA solution drop by drop in the chitosan solution, under constant agitation, resulting in nanoparticles of comparable size (Gaspar et al., 2011).

The variation of nanoparticles size increased with molecular weight of the polymer as well as PDI variation, in contrast with the decrease on the zeta potential variation. It is noteworthy that HMW chitosan provided nanoparticles with the highest zeta potential (+32.0 mV) and 5 kDa chitosan enabled nanoparticles with the lowest size (74.82 nm), both with suitable PDIs.

Table 7 presents multiple regression equations and the surface response model chosen for each output of each chitosan polymer. These equations were provided by the Design Expert analysis and indicate the level of the outputs as a function of different inputs, where the signal behind each factor represents a positive or a negative effect in the outputs (Ben Ali et al., 2020). Factor A represents the chitosan concentration and factor B represents the TPP concentration. Concerning the nanoparticle size output, Table 7 shows that the increment of chitosan concentration input had a positive effect in both LMW and 5 kDa chitosan polymers. On the other hand, the increment

of TPP concentration negatively influenced the size of nanoparticles prepared for almost all polymers, HMW chitosan being the exception. On the one hand, this behaviour of each isolated output shows that the increase of chitosan concentration implies more positive chain polymers to easily condense the same amount of negatively charged molecules (pDNA and TPP) (Fan et al., 2012), while on the other hand, the increase of TPP concentration weakens the condensation power of the same amount of chitosan polymer. In addition, for PDI and zeta potential outputs, it is evident that the chitosan concentration input induced a positive effect in almost all chitosan polymers and the TPP concentration input had a negative effect. This negative impact of the TPP can be explained by the increase of negative charges of this crosslinker in the formulation process. In addition, the increment of TPP concentration should be controlled because it can be related to aggregation phenomena (Bravo-Anaya et al., 2019; Deng et al., 2018). As evidenced in Table 7, when the surface response model chosen is quadratic, the respective output regression equation presents more information related to the input interactions (AB) and the input effect on itself (A² or B²), while the linear model only presents information of each isolated input.

Table 7: Coded multiple regression equations for each output assessed in the chitosan nanosystems formulation.

Chitosan Polymers	Output	Multiple Regression Equations	Surface Response Model
	Size	+171.00 - 8.83 A + 45.33 B	Linear
HMW Chitosan	PDI	+0.21 + 0.027 A - 0.022 B + 0.070 A ² - 5.000 E - 003 B ²	Quadratic
	Zeta potential	+26.76 + 7.59 A - 2.61 B + 2.11 AB - 4.55 A ² + 0.45 B ²	Quadratic
	Size	+96.05 + 11.34 A - 8.96 B + 0.95 AB + 5.36 A ² + 5.99 B ²	Quadratic
LMW Chitosan	PDI	+0.26 + 0.033 A - 0.058 B - 0.030 AB + 0.016 A ² + 0.059 B ²	Quadratic
	Zeta potential	+15.87 + 4.68 A - 3.86 B + 1.27 AB + 2.97 A ² + 1.02 B ²	Quadratic
	Size	+101.49 - 13.50 A - 10.77 B + 2.76 AB + 11.11 A ² + 0.11 B ²	Quadratic
20 kDa Chitosan	PDI	+0.29 - 0.027 A - 0.054 B	Linear
	Zeta potential	+ 17.35 + 2.52 A - 3.15 B	Linear
	Size	+ 77.26 + 2.15 A - 3.34 B - 12.06 AB + 9.67 A ² + 8.10 B ²	Quadratic
5 kDa Chitosan	PDI	+ 0.23 + 0.033 A - 0.054 B	Linear
	Zeta potential	+18.79 + 2.65 A - 2.97 B	Linear

The data represented in Tables 8 and 9 correspond to the statistical coefficients and the analysis of the variance (ANOVA) of four DoE, respectively, and allow to assess the goodness of fit. Based on the parameters of Tables 8 and 9, it was possible to evaluate the significance and adequacy of the used models, and to understand if these experiments were valid and fit the data through the statistical models generated. In order to evaluate if the model has high significance and the fitness of the output statistical model to the data, the coefficient of determination (R^2) has to be close to 1 (Sousa et al., 2019). In general, the R^2 values obtained in all outputs of studied chitosan polymers were around 0.9, suggesting that all models fit the data. However, the values of R^2 for PDI output of the 20 and 5 kDa chitosan polymers were 0.62 and 0.82, respectively, which indicates the polynomial model is not a good predictor of this response. This result can be related with the absence of a tendency of this response observed in Table 2 (as it was already previously described), but the obtained results (PDI below 0.4) are suitable since we intend to get homogeneous samples (Delan et al., 2020). Adjusted R^2 values indicate if the theoretical values adjust to the experimental data and should not be lower than 0.2 from its R^2 to indicate that the sample size was adequate for the model (Valente et al., 2019). Results from Table 8 show that all values of adjusted R^2 follow the same tendency of R^2 and never lower more than 0.09 in comparison to its R^2 . The predicted R^2 gives information regarding the predictive power of these models. As the results of predicted R^2 presented in Table 8 are all positive, it confirms the model's capacity in predicting new data. Lastly, adequate precision values are presented in Table 8, measuring the signal due to the noise ratio. These values must be greater than 4 to consider that the model provides an adequate signal and can be used to navigate the design space (Carlson, 2001). All adequate precision results were higher than 7.6, confirming an adequate signal-to-noise ratio. The study of all these coefficients shows that the quadratic and linear models chosen in each output (Table 8) were adequate for the statistical analysis of these results.

Table 8: Statistical coefficients obtained by the DoE for all chitosan polymers.

Chitosan Polymers	Output	R^2	R^2 Adjusted	R^2 Predicted	Adequate Precision
HMW Chitosan	Size	0.7610	0.7013	0.4895	9.255
	PDI	0.9494	0.8988	0.5463	12.978
	Zeta potential	0.9637	0.9274	0.6932	14.865
LMW Chitosan	Size	0.9577	0.9154	0.5900	15.212
	PDI	0.9484	0.8969	0.5789	13.512
	Zeta potential	0.9945	0.9891	0.9686	43.376
20 kDa Chitosan	Size	0.9598	0.9196	0.7182	15.572
	PDI	0.6282	0.5352	0.3147	7.695
	Zeta potential	0.9229	0.9036	0.8315	21.500
5 kDa Chitosan	Size	0.9741	0.9482	0.7756	18.732
	PDI	0.8201	0.7752	0.5989	12.971
	Zeta potential	0.9249	0.9061	0.8681	21.915

Table 9: ANOVA p-values for central composite design for the formulation of chitosan nanosystems.

Chitosan Polymers	Source	Size	PDI	Zeta Potential
HMW Chitosan	Model	0.0033	0.0030	0.0013
	A	0.3626	0.0066	0.0002
	B	0.0011	0.0150	0.0184
	AB	-----	1.0000	0.0720
	A ²	-----	0.0006	0.0114
	B ²	-----	0.6093	0.7132
	Lack of fit	0.0504	0.2676	0.1276
LMW Chitosan	Model	0.0019	0.0031	<0.0001
	A	0.0006	0.0131	<0.0001
	B	0.0017	0.0012	<0.0001
	AB	0.6225	0.0365	0.0050
	A ²	0.0649	0.2788	0.0003
	B ²	0.0462	0.0069	0.0288
	Lack of fit	0.1448	0.2565	0.4143
20 kDa Chitosan	Model	0.0017	0.0191	<0.0001
	A	0.0006	0.1431	0.0003
	B	0.0016	0.0109	<0.0001
	AB	0.2509	-----	-----
	A ²	0.0088	-----	-----
	B ²	0.9697	-----	-----
	Lack of fit	0.1582	0.7251	0.4872
5 kDa Chitosan	Model	0.0006	0.0010	<0.0001
	A	0.0944	0.0140	0.0002
	B	0.0240	0.0009	<0.0001
	AB	0.0002	-----	-----
	A ²	0.0018	-----	-----
	B ²	0.0039	-----	-----
	Lack of fit	0.2601	0.3772	0.2739

ANOVA analysis was performed to further prove the validity of each DoE. The results shown in Table 9 represent the model significance for each output and the correspondent lack of fit. To have a good valid model, a significant value for the model (p-value < 0.05) and a non-significant value for the lack of fit (p-value > 0.05) is necessary (Sousa et al., 2020). When the model respects these parameters, it indicates that the model data are significant and fit. According to the p-values presented in Table 9, all the model values were significant and do not present a significant lack of fit. With this data analysis, it can be confirmed that the statistical model is good and valid for all outputs. In addition, Table 9 also shows that inputs had a significant influence on all outputs, except for the chitosan concentration in the nanoparticles prepared using HMW and 5 kDa polymers and in the PDI of 20 kDa polymer.

After the statistical analysis of the coefficients, the analysis of the variance and validating the statistical models of the DoE, the Design-Expert software predicted the optimal points to the four chitosan polymers. Table 10 represents the concentration of each factor A and B (chitosan concentration and TPP concentration) that was required to obtain the optimal formulation of nanoparticles with each polymer, as well as predicted outputs and a range of values for the validation of each output (95% of confidence interval). The concentration of each factor to perform the optimal formulation was predicted, aiming at chitosan nanoparticles with the smallest size, highest zeta potential and a PDI below 0.4. These predicted values were based on inputs and experiments previously performed, and as expected, each predicted optimal point has different input conditions since results of Table 2 are strongly dependent on the applied polymer. Thus, using the chitosan concentration of 0.51 mg/mL and TPP concentration of 0.25 mg/mL with HMW chitosan, the outputs predict nanoparticles with size of 125.28 nm, zeta potential of +30.1 mV and PDI of 0.228; using the chitosan concentration of 0.2 mg/mL and TPP concentration of 0.41 mg/mL with the LMW chitosan, the outputs predict nanoparticles with size of 94.25 nm, zeta potential of +16.1 mV and PDI of 0.256; using the chitosan concentration of 0.8 mg/mL and TPP concentration of 0.34 mg/mL with 20 kDa chitosan, the outputs predict nanoparticles with size of 104.31 nm, zeta potential of +21.9 mV and PDI of 0.299 and using the chitosan concentration of 0.56 mg/mL and TPP concentration of 0.41 mg/mL with 5 kDa chitosan, the outputs predict nanoparticles with size of 81.27 nm, zeta potential of +20.4 mV and PDI of 0.257. These optimal formulations were performed, and the mean of each obtained output results from three independent experiments, being the data presented in Table 10. All polymers achieved a result within the confidence interval provided by the Design-Expert software, concluding that all the outputs are valid.

Table 10: Optimal points for the four chitosan polymers. (n =3 ± SD)

Chitosan Polymers	Predicted Input	Output	Predicted Mean	95% CI Low for Mean	95% CI High for Mean	Obtained Mean
HMW Chitosan	A(chitosan) = 0.51	Size (nm)	125.28	99.03	151.53	139.2 ± 0.76
	B(TPP) = 0.25	PDI	0.228	0.200	0.250	0.246 ± 0.01
		Zeta potential (mV)	30.1	26.7	33.5	26.8 ± 0.6
LMW Chitosan	A(chitosan) = 0.20	Size (nm)	94.25	87.68	100.83	97.82 ± 0.17
	B(TPP) = 0.41	PDI	0.256	0.220	0.29	0.223 ± 0.012
		Zeta potential (mV)	16.1	15.1	17.1	15.9 ± 0.1
20 kDa Chitosan	A(chitosan) = 0.80	Size (nm)	104.31	96.46	112.16	97.67 ± 1.48
	B(TPP) = 0.34	PDI	0.299	0.250	0.350	0.271 ± 0.006
		Zeta potential (mV)	21.9	20.6	23.2	21.8 ± 0.5
5 kDa Chitosan	A(chitosan) = 0.56	Size (nm)	81.27	78.03	84.52	81.66 ± 1.00
	B(TPP) = 0.41	PDI	0.257	0.240	0.280	0.245 ± 0.015
		Zeta potential (mV)	20.4	19.6	21.2	19.8 ± 1.1

Comparing the results of the four optimal points, the HMW chitosan resulted in nanoparticles with the highest zeta potential (+26.8 mV) but also the largest size (139.20 nm), as expected. However, 20 and 5 kDa chitosan polymers gave rise to nanoparticles of reasonable zeta potential and the size was smaller than the one achieved with HMW chitosan. 5 kDa chitosan polymer led to nanoparticles with the smaller size (81.66 nm) of four polymers. The lowest zeta potential corresponded to LMW chitosan (15.9 mV), although the size was equivalent to the nanoparticles obtained using 20 kDa chitosan. The PDI achieved for all polymers was about the same (0.22–0.26), confirming that all formulations were homogeneous. These results are consistent with previous works. Huang and co-workers achieved LMW chitosan nanoparticles with size of 94 nm, zeta potential of +5.71 mV and PDI of 0.278 (Morris et al., 2011). Although the size of LMW chitosan nanoparticles in this experiment increased by 4 nm, PDI decreased, and zeta potential is much more positive (+15.9 mV) than the nanoparticles presented by the previous work. In another work using LMW chitosan, nanoparticles with average size of 108 nm and a zeta potential of +6 mV were formulated (Shi et al., 2011). The nanoparticles obtained in the present work have a smaller size (97.82 nm) and a bigger zeta potential (+15.9 mV), which can be related to the different used formulation method or the application of the DoE tool. While nanoparticles prepared with HMW chitosan presented an average size of 181 nm and zeta potential of 22.2 mV (M. Huang et al., 2005). Özbaş-Turan and co-workers also tested the formulation of nanoparticles with HMW chitosan, but without the DoE and the resultant size remained above 190 nm (Özbaş-Turan & Akbuğa, 2011). Supported by DoE tool, nanoparticles obtained in the present work with the HMW chitosan are smaller (139.2 nm) and also more positively charged (+26.8 mV) than the presented formerly. Thus, the present work shows that DoE can be universally applied to optimize

the formulation of nanoparticles to deliver DNA by using whatever material compared to the common random experiment approach (Yan et al., 2020). Deng and co-workers produced nanoparticles based on 5 kDa chitosan with size of 144.8 nm and a zeta potential of +28 mV (Deng et al., 2018). Their studies explored chitosan/hyaluronic acid to form nanoparticles, while in our study, chitosan/TPP was used, which can explain the difference in size, given the TPP is a stronger crosslinker, creating smaller nanoparticles (81.66 nm). However, the use of TPP can be responsible for the decrease of zeta potential (19.8 mV) due to the increment of the global negative charge of pDNA solution.

This study of experimental design for the optimization of the formulation of nanoparticles from different chitosan polymers was successfully achieved. It was possible to notice differences in the outputs, between chitosan polymers with different molecular weights, mainly in terms of nanoparticles' size and charge, both parameters being higher for longer polymer chains. Additionally, the concentration of chitosan and TPP have a strong influence on these outputs. In addition, nanoformulations obtained with the four polymers analysed by SEM showed spherical or oval morphology (data not shown). This study demonstrates that it is possible to form nanoparticles with chitosan polymers of different molecular weight and improve their performance by choosing the right chitosan and TPP concentrations. This optimization process becomes extremely relevant when developing a delivery system for cellular transfection, aiming for therapeutic gene expression. The cellular up-take/internalization is favoured by carriers exhibiting a spherical morphology, small size (<200 nm), monodispersity and high positive surface charges (Foroozandeh & Aziz, 2018; Manzanares & Ceña, 2020; Rasmussen et al., 2020).

Therefore, this kind of DoE study enabled us to have a deep control over the characteristics of the formed delivery systems, thus, potentiating the desired therapeutic response.

4.3. Properties of the chitosan nanoparticles

After the process of optimization, the optimal points to formulate the nanoparticles for each polymer were defined. To evaluate the nanoparticles properties created by each polymer, some tests were performed. SEM analysis was performed to evaluate the morphology, Fourier transform infrared spectroscopy was utilized to evaluate the chemical properties, different stability assays to evaluate the endurance and DNA release, and lastly cytotoxicity assays was performed to ensure the biocompatibility of chitosan nanoparticles.

4.3.1. SEM

In order to evaluate the nanoparticles morphology, samples of each optimal point were prepared for a SEM analysis. Nanoparticles obtained with the four polymers are represented in Figure 10: A represent nanoparticles of 5 kDa chitosan, B represent nanoparticles of 20 kDa chitosan, C represent nanoparticles of LMW chitosan and D represent nanoparticles of HMW chitosan. Through the obtained images (Figure 10), it was observed that all polymers originate nanoparticles with a spherical or oval morphology. According to Chithrani and Chan research, the

nanoparticles' morphology affects cellular uptake. Nanoparticles presenting spherical shapes, such as those obtained in this work, have a higher cellular uptake than rod-shape nanoparticles (Chithrani & Chan, 2007).

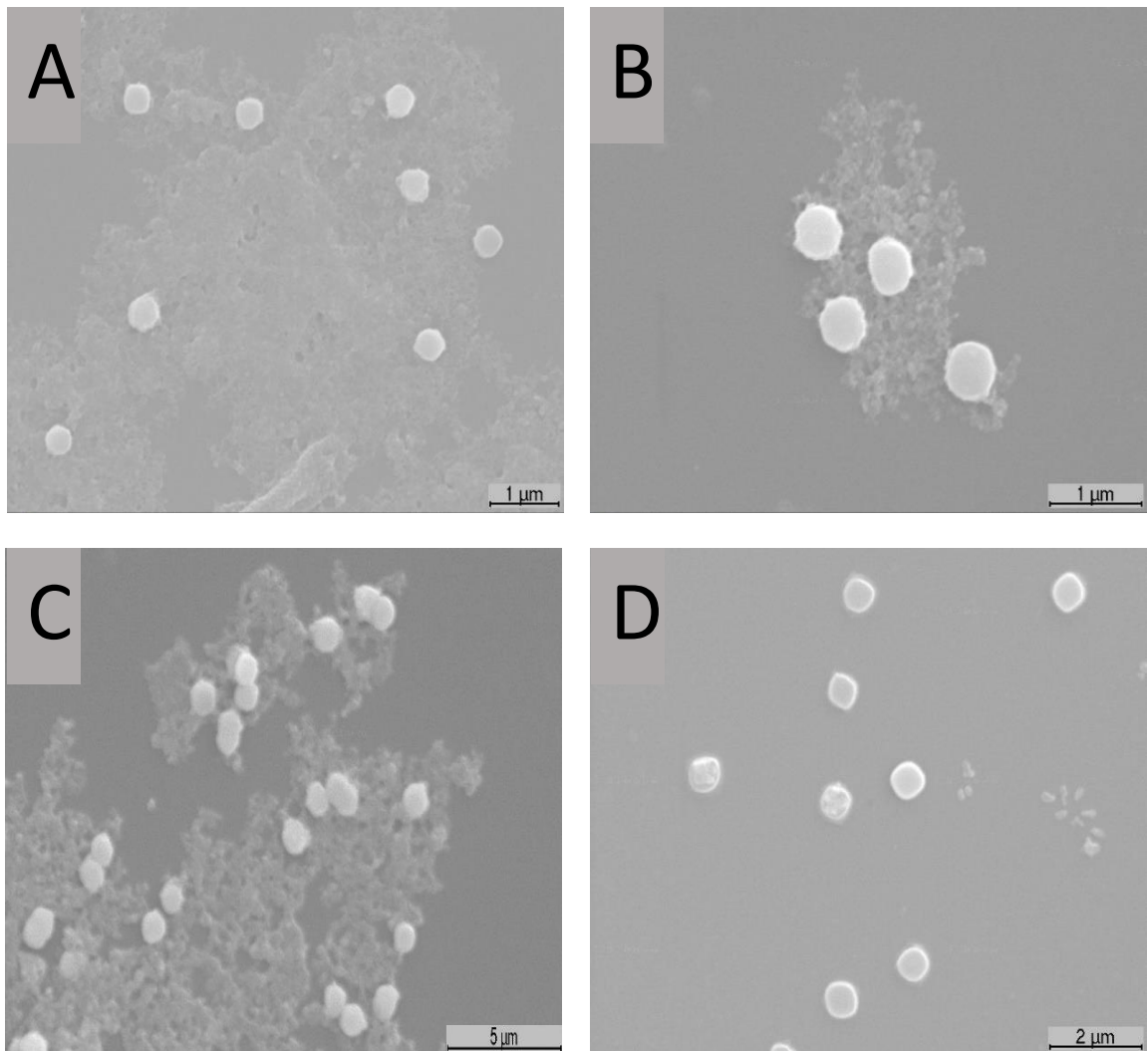


Figure 10: Nanoparticles images obtained by SEM. (A) nanoparticles of 5 kDa chitosan. (B) nanoparticles of 20 kDa chitosan. (C) nanoparticles of LMW chitosan. (D) nanoparticles of HMW chitosan.

4.3.2. Fourier Transform Infrared Spectroscopy

The FTIR technique was performed to evaluate the chemical structure of chitosan, as well as the possible interactions between pDNA and TPP. Therefore, the FTIR spectra of pDNA, TPP, HMW, LMW, 20 and 5 kDa chitosan and chitosan nanoparticles are shown in Figure 11, which reveal the fundamental absorption bands. Overall, the spectra of chitosan with different molecular weights exhibited characteristic peaks with strong similarity. The strong bands in the region 3396–3144 cm^{-1} can be attributed to N-H and O-H stretching vibrations, as well as the intramolecular hydrogen bonds. The absorption bands at 2894–2880 cm^{-1} correspond to C-H symmetric and asymmetric stretching vibrations. Bands in the region 1608–1547 cm^{-1} are related to residual N-acetyl groups in chitosan and bands between 1082 and 1074 cm^{-1} are attributed to the asymmetric stretching of the C–O–C bridge (Ibrahim et al., 2020). Similar behaviour has already been reported by previous studies, in which functional groups present in chitosan with different molecular weights were assessed (S. Chen et al., 2020; Qi et al., 2020; Song et al., 2020). Concerning the pDNA spectrum, the peaks in the region of 1700–1500 cm^{-1} correspond to the nitrogen bases. Furthermore, the peak at 1116 cm^{-1} can be assigned to the vibration of ribose (C-C sugar) and the peak at 944 cm^{-1} is indicative of the pDNA presence (Albuquerque et al., 2020). TPP spectrum demonstrated characteristic bands at 1214 cm^{-1} (P-O stretching vibration), 1084 cm^{-1} (symmetric and asymmetric stretching vibrations in PO₂ group), 973 cm^{-1} (symmetric and asymmetric stretching vibrations in PO₃ group) and 908 cm^{-1} (asymmetric stretching of the P-O-P bridge) (Loutfy et al., 2017; Tomaz et al., 2018). Regarding the spectra of chitosan/TPP/pDNA nanoparticles, a broad band in the region 3400–3200 cm^{-1} reveals enhanced intermolecular hydrogen bonding due to strong interaction bonding with TPP and pDNA. Furthermore, a new absorption peak appeared at 1414 cm^{-1} , which is assigned to N-O-P stretching vibrations. This evidence indicates that TPP anions were crosslinked with the amine groups of chitosan to form complexes, and similar results were obtained in other works (M. E. S. Ahmed et al., 2020; Loutfy et al., 2017).

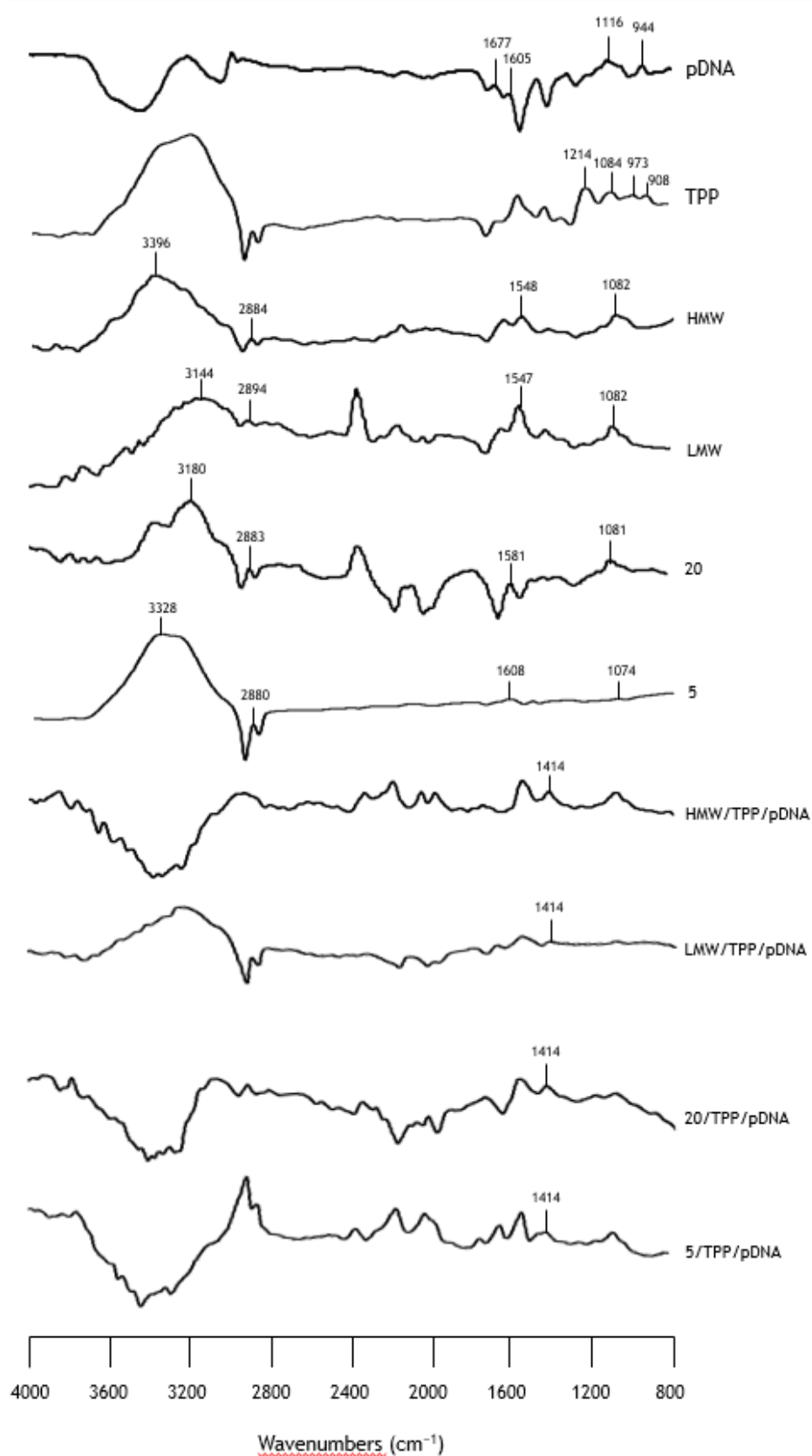


Figure 11: FTIR spectra (absorbance versus wavenumbers) of pDNA, TPP, chitosan with different molecular weights (HMW, LMW, 20 kDa, 5 kDa) and chitosan/TPP/pDNA nanoparticles.

4.3.3. Stability Assays

After establishing the optimal points for the nanoparticle's formulation with chitosan polymers of different molecular weights, it was important to evaluate nanoparticles' colloidal stability, once stored in the formulation buffer over time and at different temperatures (Jonassen et al., 2012; Morris et al., 2011; Rázga et al., 2016). Thus, the size, potential zeta and PDI of stored nanoparticles were measured after 1 h, one day, one week and one month of storage in the sodium acetate buffer (0.1 M, pH 4.6), at 4°C and room temperature. Analysing the data in Figure 12, the size of nanoparticles did not change or presented small changes over time (no more than 20 nm after one month) at 4°C for LMW, 20 and 5 kDa chitosans, always remaining near to optimal point results of the delivery systems obtained from the DoE. According to previous studies the chitosan/TPP nanoparticles only show small or moderate size changes after a month of storage at both temperatures (Jonassen et al., 2012; Morris et al., 2011; Rázga et al., 2016). These results suggest the storage conditions are suitable to avoid spontaneous aggregation, erosion of particles' spherical shape or swelling the chitosan nanoparticles, most probably by reducing the frequency of particle collisions at low temperatures (Rázga et al., 2016). These mechanisms have been responsible for the marked increase on chitosan-TPP particle size from 400 to 900 nm, after 7 days of storage. The PDI of these systems exhibit some variability over time for the four polymers, being less variable with HMW and 5 kDa chitosans. However, results indicate some homogeneity on nanoparticle size for each polymer over time, since all PDI remained below 0.4. The zeta potential of nanoparticles at room temperature was significantly reduced in all nanosystems, and this decrease ranged between 20 and 35%, depending on the polymer. Moderate changes in the zeta potential were observed when particles prepared with HMW and LMW polymers were stored at 4°C, while particles obtained with 20 and 5 kDa chitosan polymers did not show any significant changes over one month. This behaviour of HMW (200–500 kDa) and LMW (50–190 kDa) can be related to the chemical breakdown in the polymeric network of the nanoparticles obtained with polymers, which present chains with variable sizes into a specific range (Delan et al., 2020). Previous studies demonstrated that chitosan/TPP nanoparticles, after one month in deionized water, changed drastically their characteristics compared to the properties presented right after their preparation (López-León et al., 2005). This set of results suggests that the nanosystems obtained with 20 and 5 kDa chitosan polymers can be more stable than the ones formed with HMW and LMW and should be stored in the formulation buffer (acetate buffer (0.1 M, pH 4.6)) at 4 °C over time.

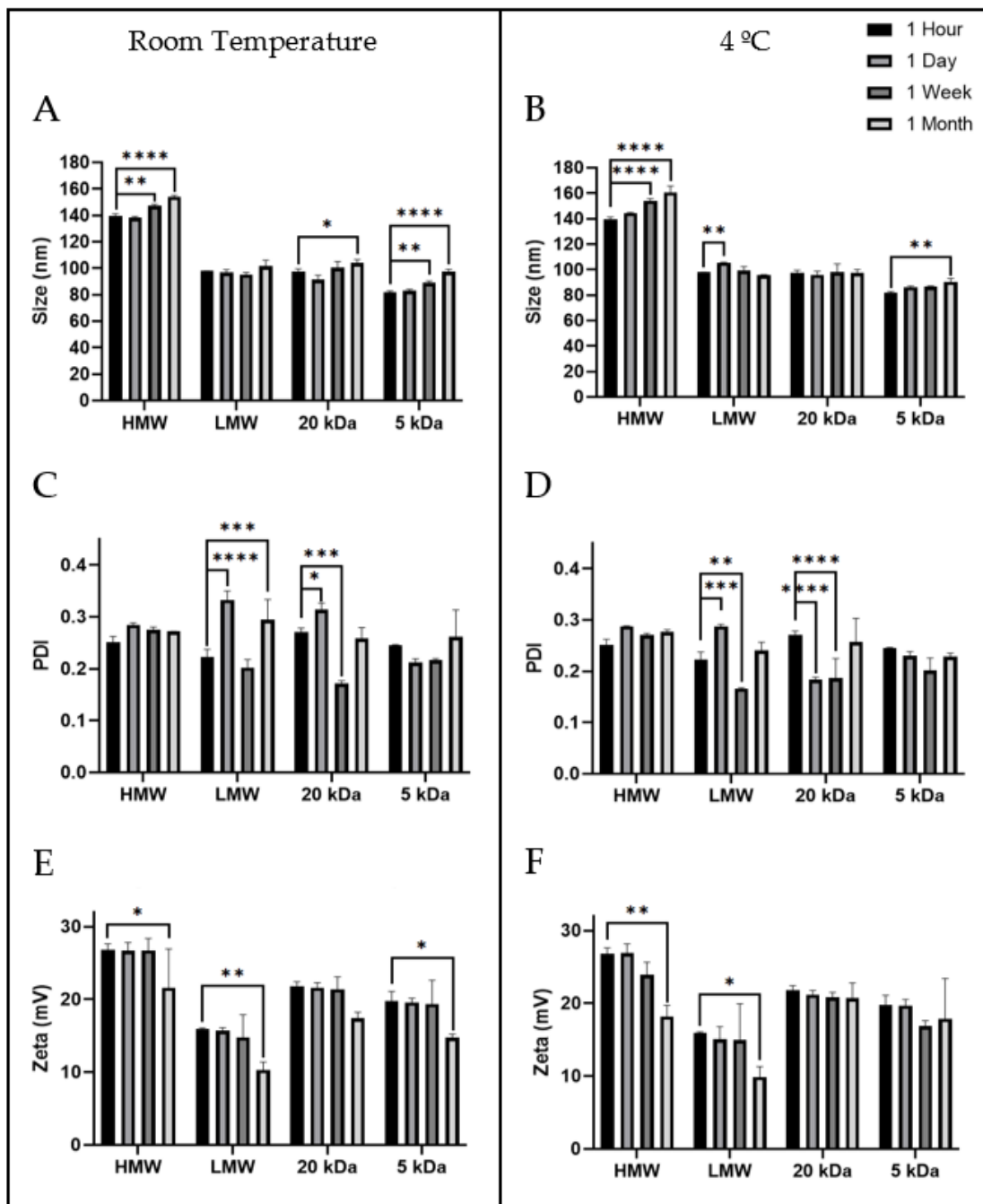


Figure 12: Stability assays of chitosan nanoparticles at 1 h, 1 day, 1 week and 1 month. (A) Chitosan nanoparticles size after storage at room temperature. (B) Chitosan nanoparticles size after storage at 4°C. (C) Chitosan nanoparticles PDI after storage at room temperature. (D) Chitosan nanoparticles PDI after storage at 4°C. (E) Chitosan nanoparticles zeta potential at room temperature. (F) Chitosan nanoparticles zeta potential at 4°C. Data obtained from three independent samples (mean \pm S.D., $n = 3$). The observed differences are statistically significant (* $p < 0.05$; ** $p < 0.01$; *** $p < 0.001$; **** $p < 0.0001$).

Furthermore, the nanoparticles stability was also evaluated following their incubation in the cell culture medium, with or without FBS supplementation, to simulate the *in vitro* cell transfection and *in vivo* extracellular conditions, to ensure the success of cellular transfection of these chitosan nanoparticles (Albuquerque et al., 2020; Serra et al., 2021). Thus, all chitosan nanoparticles were resuspended and incubated for 6 h at 37°C in two different mediums, MEM- α (normally used for dendritic cell culture) and DMEM-F12 (normally used for human fibroblast culture) with and without supplements. The supplements 10% FBS and 1% penicillin-streptomycin were subsequently added. The stability test performed in medium with supplementation aimed to mimic the extracellular environment of the human body. After 6 h, an 1% agarose gel electrophoresis was performed to monitor if the pDNA was released and degraded during the incubation process. As demonstrated in Figure 13, for both media, the different chitosan nanoparticles remained stable since it was not possible to find pDNA at the first moment of resuspension (0 h) or after 6 h of the incubation process, due to the absence of nucleic acid bands in the electrophoretic mobility profile. It is noteworthy that the presence of FBS in the medium does not have any destabilizing effect on the nanoparticles, being a good indicator of the nanoparticles resilience in the extracellular environment (Albuquerque et al., 2020; Serra et al., 2021). The effect observed in the agarose gels of Figure 13 C, D is due to the culture medium, since lane 2 corresponds only to the sample medium and presents the same aspect. In addition, chitosan nanoparticles were also decomplexated/degraded with heparin. Nanoparticles formulated by 5 kDa and 20 kDa chitosan were incubated in heparin at 60°C for 1 h. The utilization of heparin is due to the negative charge of these molecules, competing with the others polyanions to promote the degradation of the nanoparticles (Strand et al., 2010). After this incubation, an electrophoresis was performed to ensure the DNA release (Figure 14). The electrophoresis show that the DNA was released from the nanoparticles, maintaining his stability.

These results suggest that chitosan nanoparticles can efficiently protect the pDNA vector and are suitable delivery systems for DNA vaccines (Strand et al., 2010). Thus, considering the stability of chitosan nanoparticles incubated in cell culture medium and in the formulation buffer over time, *in vitro* transfection studies are essential to evaluate the biocompatibility of chitosan nanoparticles.

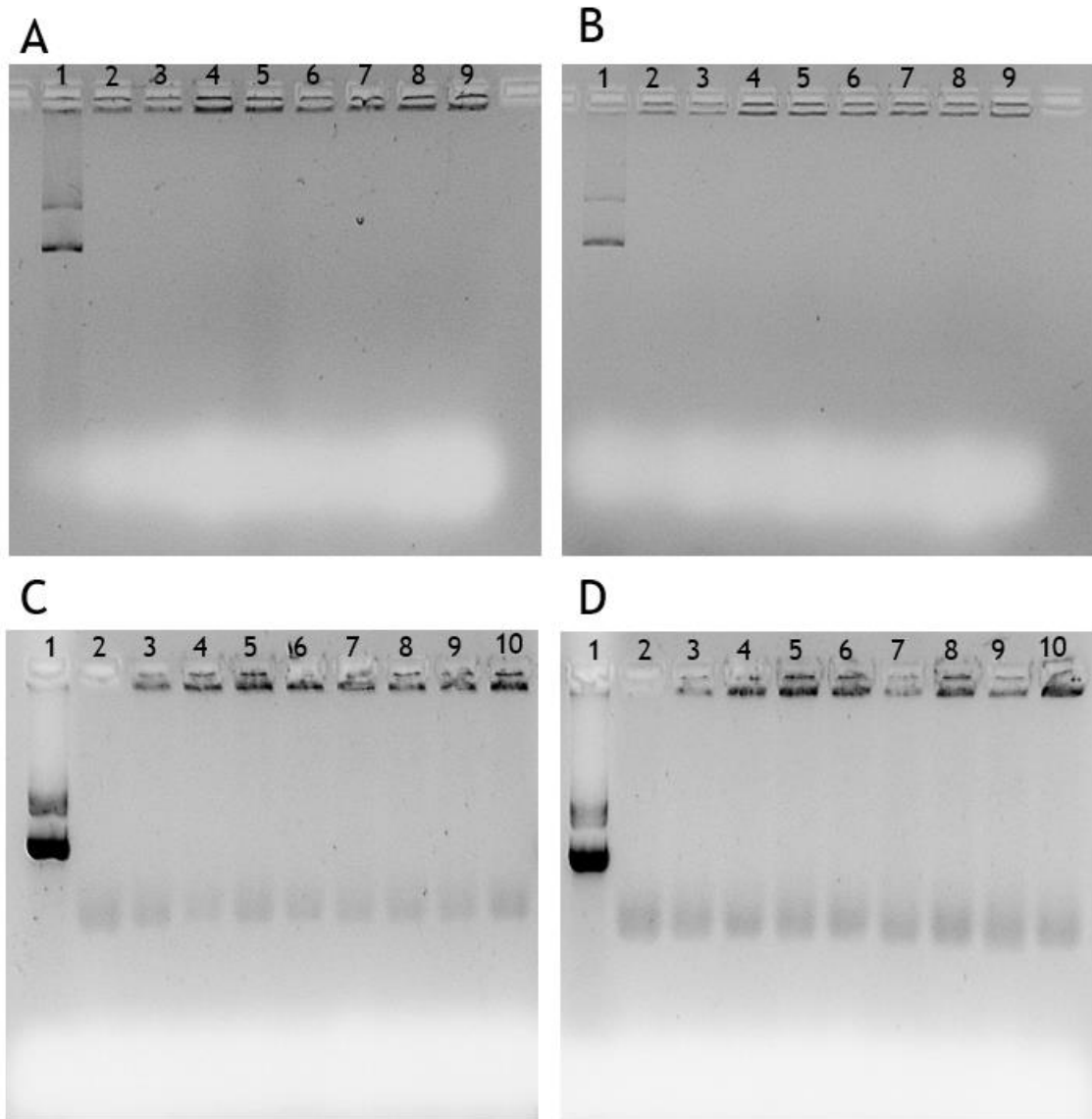


Figure 13: Analysis of nanoparticles' stability in cellular incomplete medium by agarose gel electrophoresis. Evaluation of nanoparticles stability in MEM- α incomplete medium (A) and in DMEM-F12 incomplete medium (B) at 37°C. Lane 1: pDNA E7 mut sample; lanes 2 and 3: nanoparticles obtained with HMW chitosan polymer incubated at 0 and 6 h, respectively; lanes 4 and 5: nanoparticles obtained with LMW chitosan polymer incubated at 0 and 6 h, respectively; lanes 6 and 7: nanoparticles obtained with 20 kDa chitosan polymer incubated at 0 and 6 h, respectively; lanes 8 and 9: nanoparticles obtained with 5 kDa chitosan polymer incubated at 0 and 6 h. Evaluation of nanoparticles stability in MEM- α complete medium (C) and in DMEM-F12 complete medium (D) at 37 °C. Lane 1: pDNA E7mut sample; lane 2: culture medium sample; lanes 3 and 4: nanoparticles obtained with HMW chitosan polymer incubated at 0 and 6 h, respectively; lanes 5 and 6: nanoparticles obtained with LMW chitosan polymer incubated at 0 and 6 h, respectively; lanes 7 and 8: nanoparticles obtained with 20 kDa chitosan polymer incubated at 0 and 6 h; lanes 9 and 10: nanoparticles obtained with 5 kDa chitosan polymer at 0 and 6 h.

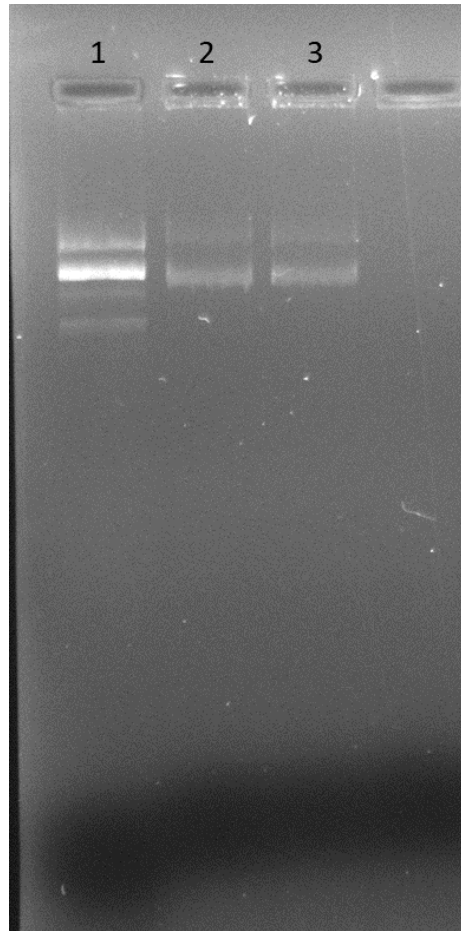


Figure 14: Electrophoretic analysis of the nanoparticles after 1 h incubation with heparin. Lane 1: pDNA E7 mut sample; lane 2: 5 kDa chitosan nanoparticles after the incubation; lane 3: 20 kDa chitosan nanoparticles after the incubation.

4.3.4. Cytotoxicity Assays

A cytotoxicity assay was performed to evaluate the biocompatibility of formulated chitosan nanoparticles. The addition of resazurin to the transfected cells determines if the chitosan systems had any toxic effects on them, through the analysis of resorufin fluorescence produced (J. L. Chen et al., 2018). As DNA vaccines require the expression of pDNA encoding antigens by APCs to induce immune responses, JAWSII cells were included in this study, which are known as difficult to transfect (Park & Bryers, 2013; Xu et al., 2016). To guarantee the safety of this approach towards other cell lines, human fibroblast cells were selected since they are widely used in cell culture. Thus, the results on JAWSII and human fibroblast cells at 48 and 72 h after transfection with the different chitosan/TPP/pDNA systems and naked DNA are presented in Figure 15. In the human fibroblasts, the chitosan polymers with the best cell viability were 5 kDa, 20 kDa and HMW, with a 99 % of cell viability and the polymer with the lower cell viability was the LMW with 98% after 48 h. The results after 72 h-have some changes, with the HMW chitosan having the lowest cell viability, of 90%, and the LMW having a cell viability of 92%, the same as 5 and 20 kDa chitosan polymers. Results show that chitosan does not have a toxic effect to human fibroblast cells, which has however shown a slight decrease with time, especially for the HMW chitosan. For

JAWSII cells, HMW and 20 kDa are the chitosan polymers that led to the highest cell viability of 98%, LMW chitosan has 96%, while the 5 kDa presented the lowest cell viability with 95% after 48 h. After 72 h, the results of cell viability were very similar for nanoparticles prepared using HMW, LMW and 20 kDa chitosan with 95% and 5 kDa with 94 %. The results indicate that the chitosan polymers do not have a toxic effect for JAWSII cells. For both cell lines, it was observed that chitosan nanoparticles did not show toxic effects since the cell viability was always superior to 90%. Similar findings were described by Hallaj-Nezhadi and co-workers, where chitosan-DNA nanoparticles showed no cell toxicity in murine CT-26 colon carcinoma cells, exhibiting average cell viabilities over 90% (Hallaj-Nezhadi et al., 2011). Therefore, the formulated delivery systems were not toxic to cells at 48 and 72 h after transfection. Furthermore, no significant differences were observed in the cell viability profile between the different chitosan systems. In contrast, cells transfected with naked DNA had a significant influence on cell viability when compared to non-transfected cells. This data demonstrates that the chitosan nanoparticles help in the delivery of the pDNA to the cells, avoiding the pDNA degradation and toxicity to the cells. These results suggest an improvement in biocompatibility when chitosan/TPP/pDNA systems were used compared to the delivery of the pDNA-E7mut vaccine alone.

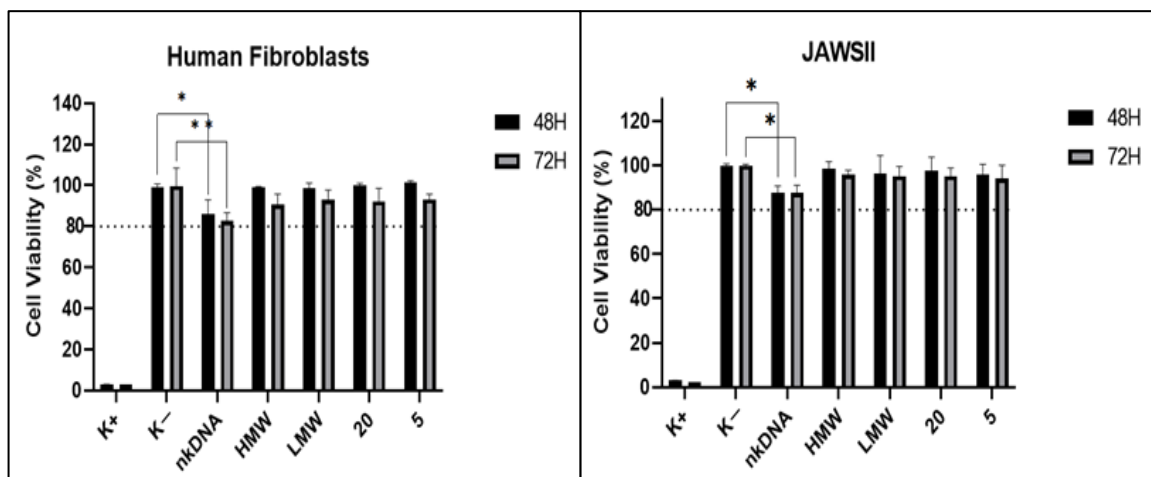


Figure 15: Cellular viability of JAWSII and human fibroblasts cells at 48 and 72 h after transfection with the different chitosan/TPP/pDNA systems and naked DNA. Cells treated with 70% ethanol were used as positive control (K+) and non-transfected cells were used as negative control (K-). The percent cell viability is expressed relative to the negative control. Data obtained from three in-dependent measurements (mean \pm S.D., n = 3). The difference between negative control and naked DNA is statistically significant (* p < 0.05; ** p < 0.01).

Chapter 5 – Conclusions and future perspectives

Although some countries have improved the prevention and screening of HPV infection and consequently decreased cervical cancer incidence, in low income countries it remains an uncontrolled problem. The development of new techniques and new tools to provide a better response, not only against this type of cancer but against all cancers in general, is essential. The study and development of therapeutic DNA vaccines against HPV can be used as a powerful tool in the fight against this cancer. DNA vaccines can produce an immune response capable to prevent a future infection but also an immune response to control and eliminate a pre-established infection. In other words, these vaccines have a preventive and a therapeutic effect, unlike conventional vaccines that only have a preventive effect.

This work was focused on the study and development of a delivery system suitable to protect, carry and deliver a DNA vaccine, in order to ensure the efficiency and maximize the immune response expected by these vaccines. Four chitosan polymers (HMW, LMW, 20 and 5 kDa) displaying different molecular weights were studied and optimized through a DoE tool. The properties (size, zeta potential, PDI, stability and cytotoxicity) of the chitosan/TPP/pDNA delivery systems were evaluated and the optimal point of nanosystems formulation was successfully achieved for each chitosan polymer used. Despite the molecular weight differences, the optimal point of formulations was achieved by the simultaneous combination of chitosan and TPP concentrations. However, each polymer resulted in formulations with different characteristics. HMW chitosan produced the highest delivery systems size (139.20 nm) and the highest zeta potential (+26.8 mV), while the 5 kDa chitosan led to the delivery systems with the smallest size (81.66 nm) and a reasonable zeta potential (+19.8 mV). The LMW and 20 kDa chitosans generated delivery systems with sizes of 97.82 and 97.67 nm and zeta potentials of +15.9 and 21.8 mV, respectively. Cytotoxicity assays revealed that none of the chitosan formulations had a toxic effect on the human fibroblasts or JAWSII cells. Stability studies concluded that the delivery systems are more stable when stored at 4°C for a month in sodium acetate buffer.

The results obtained in this master research project, showed that chitosan/TPP nanoparticles formulated by ionotropic gelation technique can create suitable delivery systems to be used in DNA vaccines, being necessary the optimization of chitosan and TPP proportions. The DoE also revealed as potent tool to achieve the optimal points for all the polymers in an easy and effective way.

However, after attaining the best formation conditions of these delivery systems, further studies can be considered to evaluate the behaviour of each formulation in *in vitro* transfection studies. Some studies point out that difference on the molecular weight can have influence in the

transfection efficiency and pDNA release. Thus, to study the efficiency of cell internalization, the pDNA can be stained with a fluorescent probe to follow the behaviour of nanosystems by confocal microscopy using live cell imaging. To evaluate the transfection efficiency, the E7 mRNA transcripts can be assessed by real time PCR and the E7 antigen expression can be proved by western blot. In addition, the delivery systems can be conjugated with some ligands, for example mannose that are recognized by receptors over expressed on the surface of antigen presenting cells, helping the nanosystems to improve targeting capabilities to the target cells (Serra et al., 2021).

Chapter 6 – References

- Adjei Boakye, E., Tobo, B. B., Rojek, R. P., Mohammed, K. A., Geneus, C. J., & Osazuwa-Peters, N. (2017). Approaching a decade since HPV vaccine licensure: Racial and gender disparities in knowledge and awareness of HPV and HPV vaccine. *Human Vaccines and Immunotherapeutics*, 13(11), 2713–2722. <https://doi.org/10.1080/21645515.2017.1363133>
- Ahmed, M. E. S., Mohamed, H. M., Mohamed, M. I., & Kandile, N. G. (2020). Sustainable antimicrobial modified chitosan and its nanoparticles hydrogels: Synthesis and characterization. *International Journal of Biological Macromolecules*, 162, 1388–1397. <https://doi.org/10.1016/j.ijbiomac.2020.08.048>
- Ahmed, T. A., & Aljaeid, B. M. (2016). Preparation, characterization, and potential application of chitosan, chitosan derivatives, and chitosan metal nanoparticles in pharmaceutical drug delivery. *Drug Design, Development and Therapy*, 10, 483–507. <https://doi.org/10.2147/DDDT.S99651>
- Albuquerque, T., Faria, R., Sousa, Â., Neves, A. R., Queiroz, J. A., & Costa, D. (2020). Polymer-peptide ternary systems as a tool to improve the properties of plasmid DNA vectors in gene delivery. *Journal of Molecular Liquids*, 309. <https://doi.org/10.1016/j.molliq.2020.113157>
- Almeida, A. M., Queiroz, J. A., Sousa, F., & Sousa, Â. (2019). Cervical cancer and HPV infection: ongoing therapeutic research to counteract the action of E6 and E7 oncoproteins. *Drug Discovery Today*, 24(10), 2044–2057. <https://doi.org/10.1016/j.drudis.2019.07.011>
- Almeida, A. M., Tomás, J., Pereira, P., Queiroz, J. A., Sousa, F., & Sousa, Â. (2018). HPV-16 targeted DNA vaccine expression: The role of purification. *Biotechnology Progress*, 34(2), 546–551. <https://doi.org/10.1002/btpr.2603>
- Ben Ali, R., Ben Ouada, S., Leboulanger, C., Ammar, J., Sayadi, S., & Ben Ouada, H. (2020). Bisphenol A removal by the Chlorophyta *Picocystis* sp.: optimization and kinetic study. *International Journal of Phytoremediation*, 0(0), 1–11. <https://doi.org/10.1080/15226514.2020.1859985>
- Bravo-Anaya, L. M., Fernández-Solís, K. G., Rosselgong, J., Nano-Rodríguez, J. L. E., Carvajal, F., & Rinaudo, M. (2019). Chitosan-DNA polyelectrolyte complex: Influence of chitosan characteristics and mechanism of complex formation. *International Journal of Biological Macromolecules*, 126, 1037–1049. <https://doi.org/10.1016/j.ijbiomac.2019.01.008>
- Bruinsmann, F. A., Pigana, S., Aguirre, T., Souto, G. D., Pereira, G. G., Bianchera, A., Fasiolo, L. T., Colombo, G., Marques, M., Pohlmann, A. R., Guterres, S. S., & Sonvico, F. (2019). Chitosan-coated nanoparticles: Effect of chitosan molecular weight on nasal transmucosal delivery. *Pharmaceutics*, 11(2), 1–19. <https://doi.org/10.3390/pharmaceutics11020086>
- Canfell, K. (2019). Towards the global elimination of cervical cancer. *Papillomavirus Research*, 8(June), 100170. <https://doi.org/10.1016/j.pvr.2019.100170>
- Carlson, R. (2001). Design of Experiments, Principles and Applications, L. Eriksson, E. Johansson, N. Kettaneh-Wold, C. Wikström and S. Wold, Umetrics AB, Umeå Learnways AB, Stockholm, 2000, ISBN 91-973730-0-1, xii + 329 pp. *Journal of Chemometrics*, 15(5), 495–496. <https://doi.org/https://doi.org/10.1002/cem.686>
- Chen, J. L., Steele, T. W. J., & Stuckey, D. C. (2018). Metabolic reduction of resazurin; location within the cell for cytotoxicity assays. *Biotechnology and Bioengineering*, 115(2), 351–358. <https://doi.org/10.1002/bit.26475>
- Chen, S., Ma, X., Han, Y., Wei, Y., Guo, Q., Yang, S., Zhang, Y., Liao, W., & Gao, Y. (2020). Effect of chitosan molecular weight on zein-chitosan nanocomplexes: Formation, characterization, and the delivery of quercetagenin. *International Journal of Biological Macromolecules*, 164, 2215–2223. <https://doi.org/10.1016/j.ijbiomac.2020.07.245>
- Chithrani, B. D., & Chan, W. C. W. (2007). Elucidating the mechanism of cellular uptake and

- removal of protein-coated gold nanoparticles of different sizes and shapes. *Nano Letters*, 7(6), 1542–1550. <https://doi.org/10.1021/nl070363y>
- de Pinho Neves, A. L., Milioli, C. C., Müller, L., Riella, H. G., Kuhnen, N. C., & Stulzer, H. K. (2014). Factorial design as tool in chitosan nanoparticles development by ionic gelation technique. *Colloids and Surfaces A: Physicochemical and Engineering Aspects*, 445, 34–39. <https://doi.org/10.1016/j.colsurfa.2013.12.058>
- Delan, W. K., Zakaria, M., Elsaadany, B., ElMeshad, A. N., Mamdouh, W., & Fares, A. R. (2020). Formulation of simvastatin chitosan nanoparticles for controlled delivery in bone regeneration: Optimization using Box-Behnken design, stability and in vivo study. *International Journal of Pharmaceutics*, 577(January), 119038. <https://doi.org/10.1016/j.ijpharm.2020.119038>
- Deng, R. H., Qiu, B., & Zhou, P. H. (2018). Chitosan/hyaluronic acid/plasmid-DNA nanoparticles encoding interleukin-1 receptor antagonist attenuate inflammation in synoviocytes induced by interleukin-1 beta. *Journal of Materials Science: Materials in Medicine*, 29(10), 1–10. <https://doi.org/10.1007/s10856-018-6160-3>
- Derbie, A., Mekonnen, D., Woldeamanuel, Y., Van Ostade, X., & Abebe, T. (2020). HPV E6/E7 mRNA test for the detection of high grade cervical intraepithelial neoplasia (CIN2+): A systematic review. *Infectious Agents and Cancer*, 15(1), 1–10. <https://doi.org/10.1186/s13027-020-0278-x>
- Durst, M., Gissmann, L., Ikenberg, H., & Zur Hausen, H. (1983). A papillomavirus DNA from a cervical carcinoma and its prevalence in cancer biopsy samples from different geographic regions. *Proceedings of the National Academy of Sciences of the United States of America*, 80(12 I), 3812–3815. <https://doi.org/10.1073/pnas.80.12.3812>
- El-Zein, M., Richardson, L., & Franco, E. L. (2016). Cervical cancer screening of HPV vaccinated populations: Cytology, molecular testing, both or none. *Journal of Clinical Virology*, 76, S62–S68. <https://doi.org/10.1016/j.jcv.2015.11.020>
- Fan, W., Yan, W., Xu, Z., & Ni, H. (2012). Formation mechanism of monodisperse, low molecular weight chitosan nanoparticles by ionic gelation technique. *Colloids and Surfaces B: Biointerfaces*, 90(1), 21–27. <https://doi.org/10.1016/j.colsurfb.2011.09.042>
- Foroozandeh, P., & Aziz, A. A. (2018). Insight into Cellular Uptake and Intracellular Trafficking of Nanoparticles. *Nanoscale Research Letters*, 13. <https://doi.org/10.1186/s11671-018-2728-6>
- Gaspar, V. M., Sousa, F., Queiroz, J. A., & Correia, I. J. (2011). Formulation of chitosan-TPP-pDNA nanocapsules for gene therapy Applications. *Nanotechnology*, 22(1). <https://doi.org/10.1088/0957-4484/22/1/015101>
- Hallaj-Nezhadi, S., Valizadeh, H., Dastmalchi, S., Baradaran, B., Jalali, M. B., Dobakhti, F., & Lotfipoure, F. (2011). Preparation of chitosan-plasmid DNA nanoparticles encoding interleukin-12 and their expression in CT-26 colon carcinoma cells. *Journal of Pharmacy and Pharmaceutical Sciences*, 14(2), 181–195. <https://doi.org/10.18433/j3tp4t>
- Hoppe-Seyler, K., Bossler, F., Braun, J. A., Herrmann, A. L., & Hoppe-Seyler, F. (2018). The HPV E6/E7 Oncogenes: Key Factors for Viral Carcinogenesis and Therapeutic Targets. *Trends in Microbiology*, 26(2), 158–168. <https://doi.org/10.1016/j.tim.2017.07.007>
- Huang, M., Fong, C. W., Khor, E., & Lim, L. Y. (2005). Transfection efficiency of chitosan vectors: Effect of polymer molecular weight and degree of deacetylation. *Journal of Controlled Release*, 106(3), 391–406. <https://doi.org/10.1016/j.jconrel.2005.05.004>
- Huang, T., Song, X., Jing, J., Zhao, K., Shen, Y., Zhang, X., & Yue, B. (2018). Chitosan-DNA nanoparticles enhanced the immunogenicity of multivalent DNA vaccination on mice against *Trueperella pyogenes* infection. *Journal of Nanobiotechnology*, 16(1), 1–15. <https://doi.org/10.1186/s12951-018-0337-2>
- Ibrahim, Y. H. E. Y., Regdon, G., Kristó, K., Kelemen, A., Adam, M. E., Hamedelniei, E. I., & Sovány, T. (2020). Design and characterization of chitosan/citrate films as carrier for oral

- macromolecule delivery. *European Journal of Pharmaceutical Sciences*, 146(June 2019), 105270. <https://doi.org/10.1016/j.ejps.2020.105270>
- Jhaveri, J., Raichura, Z., Khan, T., Momin, M., & Omri, A. (2021). Chitosan nanoparticles-insight into properties, functionalization and applications in drug delivery and theranostics. *Molecules*, 26(2). <https://doi.org/10.3390/molecules26020272>
- Johnson, C. A., James, D., Marzan, A., & Armaos, M. (2019). Cervical Cancer: An Overview of Pathophysiology and Management. *Seminars in Oncology Nursing*, 35(2), 166–174. <https://doi.org/10.1016/j.soncn.2019.02.003>
- Jonassen, H., Kjøniksen, A. L., & Hiorth, M. (2012). Stability of chitosan nanoparticles cross-linked with tripolyphosphate. *Biomacromolecules*, 13(11), 3747–3756. <https://doi.org/10.1021/bm301207a>
- Kessler, T. A. (2017). Cervical Cancer: Prevention and Early Detection. *Seminars in Oncology Nursing*, 33(2), 172–183. <https://doi.org/10.1016/j.soncn.2017.02.005>
- Köping-Höggård, M., Vårum, K. M., Issa, M., Danielsen, S., Christensen, B. E., Stokke, B. T., & Artursson, P. (2004). Improved chitosan-mediated gene delivery based on easily dissociated chitosan polyplexes of highly defined chitosan oligomers. *Gene Therapy*, 11(19), 1441–1452. <https://doi.org/10.1038/sj.gt.3302312>
- Koukaras, E. N., Papadimitriou, S. A., Bikiaris, D. N., & Froudakis, G. E. (2012). Insight on the formation of chitosan nanoparticles through ionotropic gelation with tripolyphosphate. *Molecular Pharmaceutics*, 9(10), 2856–2862. <https://doi.org/10.1021/mp300162j>
- Lee, J., Kumar, S. A., Jhan, Y. Y., & Bishop, C. J. (2020). *Since January 2020 Elsevier has created a COVID-19 resource centre with free information in English and Mandarin on the novel coronavirus COVID-19. The COVID-19 resource centre is hosted on Elsevier Connect, the company's public news and information. January.*
- Li, L., & Petrovsky, N. (2016). Molecular mechanisms for enhanced DNA vaccine immunogenicity. *Expert Review of Vaccines*, 15(3), 313–329. <https://doi.org/10.1586/14760584.2016.1124762>
- Liu, H., Galbraith, S. C., Ricart, B., Stanton, C., Smith-Goettler, B., Verdi, L., O'Connor, T., Lee, S., & Yoon, S. (2017). Optimization of critical quality attributes in continuous twin-screw wet granulation via design space validated with pilot scale experimental data. *International Journal of Pharmaceutics*, 525(1), 249–263. <https://doi.org/10.1016/j.ijpharm.2017.04.055>
- Lopes, A., Vandermeulen, G., & Pr eat, V. (2019). Cancer DNA vaccines: current preclinical and clinical developments and future perspectives. *Journal of Experimental and Clinical Cancer Research*, 38(1), 1–24. <https://doi.org/10.1186/s13046-019-1154-7>
- L opez-Le on, T., Carvalho, E. L. S., Seijo, B., Ortega-Vinuesa, J. L., & Bastos-Gonz alez, D. (2005). Physicochemical characterization of chitosan nanoparticles: Electrokinetic and stability behavior. *Journal of Colloid and Interface Science*, 283(2), 344–351. <https://doi.org/10.1016/j.jcis.2004.08.186>
- Loutfy, S. A., Salaheldin, T. A., Ramadan, M. A., Farroh, K. Y., Abdallah, Z. F., & Eloahed, T. Y. A. (2017). Synthesis, characterization and cytotoxic evaluation of graphene oxide nanosheets: In vitro liver cancer model. *Asian Pacific Journal of Cancer Prevention*, 18(4), 955–961. <https://doi.org/10.22034/APJCP.2017.18.4.955>
- MacLaughlin, F. C., Mumper, R. J., Wang, J., Tagliaferri, J. M., Gill, I., Hinchcliffe, M., & Rolland, A. P. (1998). Chitosan and depolymerized chitosan oligomers as condensing carriers for in vivo plasmid delivery. *Journal of Controlled Release*, 56(1–3), 259–272. [https://doi.org/10.1016/S0168-3659\(98\)00097-2](https://doi.org/10.1016/S0168-3659(98)00097-2)
- Mali, S. (2013). Delivery systems for gene therapy. *Indian Journal of Human Genetics*, 19(1), 3–8. <https://doi.org/10.4103/0971-6866.112870>
- Manzanares, D., & Ce na, V. (2020). Endocytosis: The nanoparticle and submicron nanocompounds gateway into the cell. *Pharmaceutics*, 12(4), 1–22.

- <https://doi.org/10.3390/pharmaceutics12040371>
- Mao, S., Sun, W., & Kissel, T. (2010). Chitosan-based formulations for delivery of DNA and siRNA. *Advanced Drug Delivery Reviews*, 62(1), 12–27.
<https://doi.org/10.1016/j.addr.2009.08.004>
- Mattiuzzi, C., & Lippi, G. (2019). Current Cancer Epidemiology glossary. *Journal of Epidemiology and Global Health*, 9(4), 217–222.
- Mayrand MH, Duarte-Franco E, Rodrigues I, et al. (2007). Human Papillomavirus DNA versus Papanicolaou Screening Tests for Cervical Cancer. *New England Journal of Medicine*, 687–696.
- Mohammed, M. A., Syeda, J. T. M., Wasan, K. M., & Wasan, E. K. (2017). An overview of chitosan nanoparticles and its application in non-parenteral drug delivery. *Pharmaceutics*, 9(4). <https://doi.org/10.3390/pharmaceutics9040053>
- Morris, G. A., Castile, J., Smith, A., Adams, G. G., & Harding, S. E. (2011). The effect of prolonged storage at different temperatures on the particle size distribution of tripolyphosphate (TPP)-chitosan nanoparticles. *Carbohydrate Polymers*, 84(4), 1430–1434. <https://doi.org/10.1016/j.carbpol.2011.01.044>
- Moura, M., Marçal, G., Garcia, S., & Mendonça, M. (2020). *Since January 2020 Elsevier has created a COVID-19 resource centre with free information in English and Mandarin on the novel coronavirus COVID-19 . The COVID-19 resource centre is hosted on Elsevier Connect , the company 's public news and information . January.*
- Myers, J., Well, A., & Lorch, R. (2010). *Research Design and Statistical Analysis, Third Edition.*
- Ortega Rodríguez, N. R., Audicana Berasategui, M. T., de la Hoz Caballer, B., & Valero Santiago, A. (2021). The century of mrna vaccines: COVID-19 vaccines and allergy. *Journal of Investigational Allergology and Clinical Immunology*, 31(1), 89–91.
<https://doi.org/10.18176/jiaci.0665>
- Özbaş-Turan, S., & Akbuğa, J. (2011). Plasmid DNA-loaded chitosan/TPP nanoparticles for topical gene delivery. *Drug Delivery*, 18(3), 215–222.
<https://doi.org/10.3109/10717544.2010.544688>
- Pal, A., & Kundu, R. (2020). Human Papillomavirus E6 and E7: The Cervical Cancer Hallmarks and Targets for Therapy. *Frontiers in Microbiology*, 10(January).
<https://doi.org/10.3389/fmicb.2019.03116>
- Pan, C., Qian, J., Zhao, C., Yang, H., Zhao, X., & Guo, H. (2020). Study on the relationship between crosslinking degree and properties of TPP crosslinked chitosan nanoparticles. *Carbohydrate Polymers*, 241(February), 116349.
<https://doi.org/10.1016/j.carbpol.2020.116349>
- Park, J., & Bryers, J. D. (2013). Chemokine programming dendritic cell antigen response: Part II - programming antigen presentation to T lymphocytes by partially maintaining immature dendritic cell phenotype. *Immunology*, 139(1), 88–99. <https://doi.org/10.1111/imm.12059>
- Qi, X., Simsek, S., Ohm, J. B., Chen, B., & Rao, J. (2020). Viability of: Lactobacillus rhamnosus GG microencapsulated in alginate/chitosan hydrogel particles during storage and simulated gastrointestinal digestion: Role of chitosan molecular weight. *Soft Matter*, 16(7), 1877–1887. <https://doi.org/10.1039/c9sm02387a>
- Ramamoorth, M., & Narvekar, A. (2015). Non viral vectors in gene therapy - An overview. *Journal of Clinical and Diagnostic Research*, 9(1), GE01–GE06.
<https://doi.org/10.7860/JCDR/2015/10443.5394>
- Rasmussen, M. K., Pedersen, J. N., & Marie, R. (2020). Size and surface charge characterization of nanoparticles with a salt gradient. *Nature Communications*, 11(1), 1–8.
<https://doi.org/10.1038/s41467-020-15889-3>
- Rázga, F., Vnuková, D., Némethová, V., Mazancová, P., & Lacík, I. (2016). Preparation of chitosan-TPP sub-micron particles: Critical evaluation and derived recommendations.

- Carbohydrate Polymers*, 151, 488–499. <https://doi.org/10.1016/j.carbpol.2016.05.092>
- Rizeq, B. R., Younes, N. N., Rasool, K., & Nasrallah, G. K. (2019). Synthesis, bioapplications, and toxicity evaluation of chitosan-based nanoparticles. *International Journal of Molecular Sciences*, 20(22). <https://doi.org/10.3390/ijms20225776>
- Sadeghi, A. M. M., Dorkoosh, F. A., Avadi, M. R., Saadat, P., Rafiee-Tehrani, M., & Junginger, H. E. (2008). Preparation, characterization and antibacterial activities of chitosan, N-trimethyl chitosan (TMC) and N-diethylmethyl chitosan (DEMC) nanoparticles loaded with insulin using both the ionotropic gelation and polyelectrolyte complexation methods. *International Journal of Pharmaceutics*, 355(1–2), 299–306. <https://doi.org/10.1016/j.ijpharm.2007.11.052>
- Sadikovic, B., Al-Romaih, K., Squire, J., & Zielenska, M. (2008). Cause and Consequences of Genetic and Epigenetic Alterations in Human Cancer. *Current Genomics*, 9(6), 394–408. <https://doi.org/10.2174/138920208785699580>
- Serra, A. S., Eusébio, D., Neves, A. R., Albuquerque, T., Bhatt, H., Biswas, S., Costa, D., & Sousa, Â. (2021). Synthesis and Characterization of Mannosylated Formulations to Deliver a Minicircle DNA Vaccine. *Pharmaceutics*, 13(5), 673. <https://doi.org/10.3390/pharmaceutics13050673>
- Sharma, D., Arora, S., Singh, J., & Layek, B. (2021). A review of the tortuous path of nonviral gene delivery and recent progress. *International Journal of Biological Macromolecules*, 183(April), 2055–2073. <https://doi.org/10.1016/j.ijbiomac.2021.05.192>
- Shi, Q., Wang, H., Tran, C., Qiu, X., Winnik, F. M., Zhang, X., Dai, K., Benderdour, M., & Fernandes, J. C. (2011). Hydrodynamic delivery of chitosan-folate-DNA nanoparticles in rats with adjuvant-induced arthritis. *Journal of Biomedicine and Biotechnology*, 2011. <https://doi.org/10.1155/2011/148763>
- Shim, G., Kim, D., Le, Q.-V., Park, G. T., Kwon, T., & Oh, Y.-K. (2018). Nonviral Delivery Systems For Cancer Gene Therapy: Strategies And Challenges. *Current Gene Therapy*, 18, 3–20. <https://doi.org/10.2174/1566523218666180119121949>
- Slivac, I., Guay, D., Mangion, M., Champeil, J., & Gaillet, B. (2017). Non-viral nucleic acid delivery methods. *Expert Opinion on Biological Therapy*, 17(1), 105–118. <https://doi.org/10.1080/14712598.2017.1248941>
- Sluimer, J., & Distel, B. (2018). Regulating the human HECT E3 ligases. *Cellular and Molecular Life Sciences*, 75(17), 3121–3141. <https://doi.org/10.1007/s00018-018-2848-2>
- Song, X., Chen, Y., Zhao, G., Sun, H., Che, H., & Leng, X. (2020). Effect of molecular weight of chitosan and its oligosaccharides on antitumor activities of chitosan-selenium nanoparticles. *Carbohydrate Polymers*, 231(September), 115689. <https://doi.org/10.1016/j.carbpol.2019.115689>
- Sousa, Â., Almeida, A. M., Faria, R., Konate, K., Boisguerin, P., Queiroz, J. A., & Costa, D. (2019). Optimization of peptide-plasmid DNA vectors formulation for gene delivery in cancer therapy exploring design of experiments. *Colloids and Surfaces B: Biointerfaces*, 183(July), 110417. <https://doi.org/10.1016/j.colsurfb.2019.110417>
- Sousa, Â., Faria, R., Albuquerque, T., Bhatt, H., Biswas, S., Queiroz, J. A., & Costa, D. (2020). Design of experiments to select triphenylphosphonium-polyplexes with suitable physicochemical properties for mitochondrial gene therapy. *Journal of Molecular Liquids*, 302, 1–10. <https://doi.org/10.1016/j.molliq.2020.112488>
- Strand, S. P., Lelu, S., Reitan, N. K., de Lange Davies, C., Artursson, P., & Vårum, K. M. (2010). Molecular design of chitosan gene delivery systems with an optimized balance between polyplex stability and polyplex unpacking. *Biomaterials*, 31(5), 975–987. <https://doi.org/10.1016/j.biomaterials.2009.09.102>
- Sung, Y. K., & Kim, S. W. (2019). Recent advances in the development of gene delivery systems. *Biomaterials Research*, 23(1), 1–7. <https://doi.org/10.1186/s40824-019-0156-z>
- Surai, P. F. (2015). Silymarin as a natural antioxidant: An overview of the current evidence and

- perspectives. *Antioxidants*, 4(1), 204–247. <https://doi.org/10.3390/antiox4010204>
- Suschak, J. J., Williams, J. A., & Schmaljohn, C. S. (2017). Advancements in DNA vaccine vectors, non-mechanical delivery methods, and molecular adjuvants to increase immunogenicity. *Human Vaccines and Immunotherapeutics*, 13(12), 2837–2848. <https://doi.org/10.1080/21645515.2017.1330236>
- Székely, G., Henriques, B., Gil, M., & Alvarez, C. (2014). Experimental design for the optimization and robustness testing of a liquid chromatography tandem mass spectrometry method for the trace analysis of the potentially genotoxic 1,3-diisopropylurea. *Drug Testing and Analysis*, 6(9), 898–908. <https://doi.org/10.1002/dta.1583>
- Szymonowicz, K. A., & Chen, J. (2020). Biological and clinical aspects of HPV-related cancers. *Cancer Biology and Medicine*, 17(4), 864–878. <https://doi.org/10.20892/j.issn.2095-3941.2020.0370>
- Tiffon, C. (2018). The impact of nutrition and environmental epigenetics on human health and disease. *International Journal of Molecular Sciences*, 19(11). <https://doi.org/10.3390/ijms19113425>
- Tomaić, V. (2016). Functional roles of E6 and E7 oncoproteins in HPV-induced malignancies at diverse anatomical sites. *Cancers*, 8(10). <https://doi.org/10.3390/cancers8100095>
- Tomaz, A. F., de Carvalho, S. M. S., Barbosa, R. C., Silva, S. M. L., Gutierrez, M. A. S., de Lima, A. G. B., & Fook, M. V. L. (2018). Ionically crosslinked chitosan membranes used as drug carriers for cancer therapy application. *Materials*, 11(10), 1–18. <https://doi.org/10.3390/ma11102051>
- Torre, L. A., Siegel, R. L., Ward, E. M., & Jemal, A. (2016). Global cancer incidence and mortality rates and trends - An update. *Cancer Epidemiology Biomarkers and Prevention*, 25(1), 16–27. <https://doi.org/10.1158/1055-9965.EPI-15-0578>
- Trent, R. J. (2012). Chapter 7 - Development, Aging and Cancer. In R. J. Trent (Ed.), *Molecular Medicine (Fourth Edition)* (Fourth Edi, pp. 203–243). Academic Press. <https://doi.org/https://doi.org/10.1016/B978-0-12-381451-7.00007-4>
- Tsakogiannis, D., Gartzonika, C., Levidiotou-Stefanou, S., & Markoulatos, P. (2017). Molecular approaches for HPV genotyping and HPV-DNA physical status. *Expert Reviews in Molecular Medicine*, 19, 1–20. <https://doi.org/10.1017/erm.2017.2>
- Turcsányi, Á., Varga, N., & Csapó, E. (2020). Chitosan-modified hyaluronic acid-based nanosized drug carriers. *International Journal of Biological Macromolecules*, 148, 218–225. <https://doi.org/10.1016/j.ijbiomac.2020.01.118>
- Ura, T., Okuda, K., & Shimada, M. (2014). Developments in viral vector-based vaccines. *Vaccines*, 2(3), 624–641. <https://doi.org/10.3390/vaccines2030624>
- Valente, J. F. A., Dias, J. R., Sousa, A., & Alves, N. (2019). Composite central face design-an approach to achieve efficient alginate microcarriers. *Polymers*, 11(12). <https://doi.org/10.3390/polym11121949>
- Vannucci, L., Lai, M., Chiuppesi, F., Ceccherini-Nelli, L., & Pistello, M. (2013). Viral vectors: A look back and ahead on gene transfer technology. *New Microbiologica*, 36(1), 1–22.
- Vu, M., Yu, J., Awolude, O. A., & Chuang, L. (2018). Cervical cancer worldwide. *Current Problems in Cancer*, 42(5), 457–465. <https://doi.org/10.1016/j.currprobcancer.2018.06.003>
- Wang, J., Mamuti, M., & Wang, H. (2020). Therapeutic Vaccines for Cancer Immunotherapy. *ACS Biomaterials Science and Engineering*, 6(11), 6036–6052. <https://doi.org/10.1021/acsbiomaterials.0c01201>
- Wang, Q., Zhao, Y., Guan, L., Zhang, Y., Dang, Q., Dong, P., Li, J., & Liang, X. (2017). Preparation of astaxanthin-loaded DNA/chitosan nanoparticles for improved cellular uptake and antioxidation capability. *Food Chemistry*, 227, 9–15.










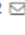

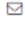



<https://doi.org/10.1016/j.foodchem.2017.01.081>

- Wang, R., Pan, W., Jin, L., Huang, W., Li, Y., Wu, D., Gao, C., Ma, D., & Liao, S. (2020). Human papillomavirus vaccine against cervical cancer: Opportunity and challenge. *Cancer Letters*, 471, 88–102. <https://doi.org/10.1016/j.canlet.2019.11.039>
- Xu, Y., Liang, W., Qiu, Y., Cespi, M., Palmieri, G. F., Mason, A. J., & Lam, J. K. W. (2016). Incorporation of a nuclear localization signal in pH responsive LAH4-L1 peptide enhances transfection and nuclear uptake of plasmid DNA. *Molecular Pharmaceutics*, 13(9), 3141–3152. <https://doi.org/10.1021/acs.molpharmaceut.6b00338>
- Yan, J., Guan, Z. Y., Zhu, W. F., Zhong, L. Y., Qiu, Z. Q., Yue, P. F., Wu, W. T., Liu, J., & Huang, X. (2020). Preparation of puerarin chitosan oral nanoparticles by ionic gelation method and its related kinetics. *Pharmaceutics*, 12(3). <https://doi.org/10.3390/pharmaceutics12030216>
- Yang, A., Farmer, E., Wu, T. C., & Hung, C. F. (2016). Perspectives for therapeutic HPV vaccine development. *Journal of Biomedical Science*, 23(1), 1–19. <https://doi.org/10.1186/s12929-016-0293-9>
- Yin, H., Kanasty, R. L., Eltoukhy, A. A., Vegas, A. J., Dorkin, J. R., & Anderson, D. G. (2014). Non-viral vectors for gene-based therapy. *Nature Reviews Genetics*, 15(8), 541–555. <https://doi.org/10.1038/nrg3763>
- Yue, Z. G., Wei, W., Lv, P. P., Yue, H., Wang, L. Y., Su, Z. G., & Ma, G. H. (2011). Surface charge affects cellular uptake and intracellular trafficking of chitosan-based nanoparticles. *Biomacromolecules*, 12(7), 2440–2446. <https://doi.org/10.1021/bm101482r>
- Zhao, D., Yu, S., Sun, B., Gao, S., Guo, S., & Zhao, K. (2018). Biomedical applications of chitosan and its derivative nanoparticles. *Polymers*, 10(4). <https://doi.org/10.3390/polym10040462>
- Zhao, F., Zhao, Y., Liu, Y., Chang, X., Chen, C., & Zhao, Y. (2011). Cellular uptake, intracellular trafficking, and cytotoxicity of nanomaterials. *Small*, 7(10), 1322–1337. <https://doi.org/10.1002/smll.201100001>

Chapter 7 – Annexes

Open Access Article

Design of Experiments to Achieve an Efficient Chitosan-Based DNA Vaccine Delivery System

by  Carlos Rodolfo ¹ ,  Dalinda Eusébio ¹ ,  Cathy Ventura ¹ ,  Renato Nunes ¹ ,
 Helena F. Florindo ² ,  Diana Costa ¹  and  Ângela Sousa ^{1,*}  

¹ CICS-UBI—Health Science Research Centre, University of Beira Interior, Av. Infante D. Henrique, 6200-506 Covilhã, Portugal

² Research Institute for Medicines (iMed.U LISBOA), Faculty of Pharmacy, Universidade de Lisboa, 1649-003 Lisbon, Portugal

* Author to whom correspondence should be addressed.

Academic Editors: Nuno Alves, Joana Valente and Alyssa Panitch

Pharmaceutics **2021**, *13*(9), 1369; <https://doi.org/10.3390/pharmaceutics13091369>

Received: 23 July 2021 / Revised: 18 August 2021 / Accepted: 28 August 2021 / Published: 31 August 2021

(This article belongs to the Special Issue Additive Manufacturing Approaches to Produce Drug Delivery Systems)

[View Full-Text](#)

[Download PDF](#)

[Browse Figures](#)

[Review Reports](#)

[Citation Export](#)

Abstract

In current times, DNA vaccines are seen as a promising approach to treat and prevent diseases, such as virus infections and cancer. Aiming at the production of a functional and effective plasmid DNA (pDNA) delivery system, four chitosan polymers, differing in the molecular weight, were studied using the design of experiments (DoE) tool. These gene delivery systems were formulated by ionotropic gelation and exploring the chitosan and TPP concentrations as DoE inputs to maximize the nanoparticle positive charge and minimize their size and polydispersity index (PDI) as DoE outputs. The obtained linear and quadratic models were statistically significant (p -value < 0.05) and non-significant lack of fit, with suitable coefficient of determination and the respective optimal points successfully validated. Furthermore, morphology, stability and cytotoxicity assays were performed to evaluate the endurance of these systems over time and their further potential for future in vitro studies. The subsequent optimization process was successfully achieved for the delivery systems based on the four chitosan polymers, in which the smallest particle size was obtained for the carrier containing the 5 kDa chitosan (~82 nm), while the nanosystem prepared with the high molecular weight (HMW) chitosan displayed the highest zeta potential (~+26.8 mV). Delivery systems were stable in the formulation buffer after a month and did not exhibit toxicity for the cells. In this sense, DoE revealed to be a powerful tool to explore and tailor the characteristics of chitosan/pDNA nanosystems significantly contributing to unraveling an optimum carrier for advancing the DNA vaccines delivery field. [View Full-Text](#)

Keywords: chitosan polymers; delivery systems; design of experiments; DNA vaccine; HPV